Electrochemistry Communications 177 (2025) 107949

Contents lists available at ScienceDirect

Electrochemistry Communications

journal homepage: www.elsevier.com/locate/elecom

Integration of the All-in-One electrode in an electrochemical flow cell for *in situ* hydrogen peroxide supply in hydroxylation mediated by immobilized unspecific peroxygenase

Giovanni V. Sayoga [a,*], Victoria S. Bueschler [a], Hubert Beisch [b], Bodo Fiedler [b], Daniel Ohde [a], Andreas Liese [a,*]

[a] Institute of Technical Biocatalysis, Hamburg University of Technology, Denickestraße 15, 21073 Hamburg, Germany
[b] Institute of Polymers and Composites, Hamburg University of Technology, Denickestraße 15, 21073 Hamburg, Germany

ARTICLE INFO

Keywords:
Biocatalysis
Bioelectrochemical system
Electrosynthesis
Flow reactor
Hydroxylation
Unspecific peroxygenase

ABSTRACT

Hydrogen peroxide (H_2O_2) is a strong oxidizing agent that is commonly employed in chemical synthesis. Nevertheless, its utilization as a cosubstrate in biocatalytic reactions remains limited due to the deactivating effect on biocatalysts at an elevated concentration. An electrochemical synthesis of H_2O_2 represents an attractive approach, offering a controllable *in situ* generation of H_2O_2 without producing complex by-products. The objective of this study is to demonstrate the feasibility of the *in situ* electrogeneration of H_2O_2 using the All-in-One (AiO) electrode within a flow reactor technology. Integrating a bioelectrochemical system (BES) into a flow reactor technology, such as a flow cell, presents an alternative strategy for scale-up. In this study, the *in situ* generation of H_2O_2 is coupled with the hydroxylation of 4-ethylbenzoic acid catalyzed by the immobilized recombinant unspecific peroxygenase from *Agrocybe aegerita* (r*Aae*UPO) within a complete BES under batch and fed-batch operation modes. The electrochemical flow cell facilitates a controllable H_2O_2 generation by adjusting experimental parameters such as current density, aeration rate and residence time. The flow cell BES equipped with the AiO electrode yielded a catalytic productivity as high as 1.24 ± 0.02 mM h^{-1} (4.95 ± 0.1 g L^{-1} $1\ d^{-1}$), a total turnover number of r*Aae*UPO up to $3.38 \cdot 10^5 \pm 702$ mol mol^{-1} and a turnover frequency up to 8.34 ± 0.14 s^{-1}.

1. Introduction

Hydrogen peroxide (H_2O_2) finds its extensive application across diverse industrial sectors, particularly in chemical synthesis [1–3], environmental remediation [4,5] and energy conversion [6]. Despite its environmentally benign properties, with water being the only degradation product [7], current large scale production methods, such as the anthraquinone oxidation (AO) process and direct synthesis from molecular H_2/O_2 gases, pose sustainability challenges [7,8]. The AO process produces by-products such as 2-ethyl-5,6,7,8-tetrahydroanthrahydroquinone, which requires additional solvent regeneration step and hydrogenation catalyst regeneration steps, as well as multi-step purification [7]. These factors contribute to the process's relatively high energy demand, estimated at approximately $16 \cdot 10^6$ J kg_{H2O2}^{-1} [9], with one study reporting an energy consumption of 17.6 kWh kg_{H2O2}^{-1} [10]. This process also generates significant waste, including toxic organic working solutions (2.5 kg t_{H2O2}^{-1}, *e.g.,* C9–C10 aromatics or 1,3,5-trimethylbenzene; due to incomplete regeneration), solid waste (15 kg t_{H2O2}^{-1}, primarily waste clay), wastewater (0.15 m^3 t_{H2O2}^{-1}), and waste gas (1.39 m^3 t_{H2O2}^{-1}) [11]. Moreover, the handling and storage of bulk H_2O_2 entail safety risks and significant costs [12], which is unjustifiable given that only certain industries, such as electronic industry for silicon etching and the aerospace industry for rocket propulsion, require the use of concentrated H_2O_2 [7,13,14]. Additionally, a direct H_2O_2 synthesis from molecular H_2 and O_2 either under plasma or utilizing noble metal catalyst such as Pd/Au suffers from critical potential explosion of H_2/O_2 gas mixture, which is flammable at 4–94 % v/v H_2 [7,15,16]. In light of these challenges, ongoing research focuses on alternative, cleaner synthesis routes for H_2O_2 [17]. This aspect is further supported considering that H_2O_2 also can be used as a cosubstrate in a

* **Corresponding authors at:** Institute of Technical Biocatalysis, Hamburg University of Technology, Denickestraße 15, 21073 Hamburg, Germany.
E-mail addresses: giovanni.sayoga@tuhh.de (G.V. Sayoga), liese@tuhh.de (A. Liese).

https://doi.org/10.1016/j.elecom.2025.107949
Received 22 December 2024; Received in revised form 11 April 2025; Accepted 30 April 2025
Available online 4 May 2025

variety of industry-relevant biocatalytic reactions [18], offering green alternative to conventional chemical processes [19], such as epoxidation [20,21], decarboxylation [22] and hydroxylation [23]. Despite its potential, the technical integration of H_2O_2 into biocatalytic systems is still limited, as high concentrations of H_2O_2 lead to rapid biocatalyst inactivation [18,24].

H_2O can be generated through two primary electrochemical pathways: (1) at the anode *via* the two-electron oxidation of water ($2H_2O \rightarrow H_2O_2 + 2H^+ + 2e^-$), or (2) at the cathode *via* the two-electron oxygen reduction reaction (ORR) ($O_2 + 2H^+ + 2e^- \rightarrow H_2O_2$) [17]. A direct *in situ* electrosynthesis of H_2O_2 at an electrode surface emerges as an appealing strategy to mitigate the irreversible enzyme deactivation [25]. This approach not only prioritizes environmental sustainability by eliminating the need for additional chemicals [26], but also facilitates precise and controllable H_2O_2 supply, thereby circumvents the risk of excessive H_2O_2 accumulation [25]. In contrast to the manual or sensor-controlled feeding of H_2O_2, *in situ* electrosynthesis of H_2O_2 maintains a constant reaction volume and prevents high local H_2O_2 concentrations [27,28]. Furthermore, it circumvents the formation of complex by-products (*e.g.,* gluconic acid) [29] and the necessity to employ additional enzymes (*e.g.,* glucose oxidase) [30] or chemicals (*e.g.,* L-ascorbic acid) to generate H_2O_2 *in situ* [31]. Additionally, its application in bioelectrochemical system (BES) facilitates a nearly CO_2 neutral chemical synthesis with an exceptional selectivity, especially through the combination of renewable energy, green biocatalysts and sustainable resources [32,33]. It is worth mentioning that recent study reported the successful application of dehydroascorbic acid (DHA)/ hydrated DHA, which is the oxidation product of ascorbate acid, as co-substrate to activate O_2 [34]. Thus, enable the H_2O_2-dependent reactions. The electrochemical *in situ* H_2O_2 generation, utilizing various electrode materials, has been already combined with biocatalytic reactions [35–37]. Specifically, this approach has been applied in the selective oxidation of thioanisole catalyzed by chloroperoxidase (CPO) [38], the synthesis of bromolactone mediated by vanadium CPO [39], and the hydroxylation of ethylbenzene catalyzed by the recombinant unspecific peroxygenase from *Agrocybe aegerita* (r*Aae*UPO) [40].

Initially developed for the *in situ* generation of hydrogen within anaerobic fermentations [41–43], the All-in-One (AiO) electrode, integrates both counter and working electrodes into a single cylindrical structure [41]. This design enables seamless integration into conventional bioreactors, effectively transforming regular bioreactors into a BES [41,42]. The implementation of the AiO electrode within an electroenzymatic process using free enzyme in a stirred tank reactor was already established [44]. Although a numbering-up approach of these electrodes could offer a higher electrode surface to volume ratio in a larger reaction volume [41], an alternative scalable strategy could be realized using flow reactors, which was not yet explored. Continuous flow synthesis in a flow reactor technology has gained attention from the chemical community, especially, due to its excellent heat and mass transfer, predictable flow behavior and suitability for sequential reactions with different substrates, thus, exhibiting high degree of reaction control [45,46]. Integrating a flow reactor technology such as flow cell into a BES, particularly for *in situ* cosubstrate generation, presents an alternate scale-up strategy. Flow cells can be numbered-up and stacked as modular units, with the number of cells increasing as the reaction volume increases. This not only combines the benefits of flow reactor technology, but also achieves a higher electrode surface to reaction volume ratio, which is important for BES.

In this study, the AiO electrode was integrated into a flow cell to generate the cosubstrate H_2O_2 *in situ*. The electrochemical flow cell with the integrated AiO electrode was connected and circulated through an enzyme reactor where the enzyme-catalyzed reaction took place, establishing an overall circulation loop reactor (Fig. 1). As a model reaction, the *in situ* electrosynthesis of H_2O_2 was combined with the

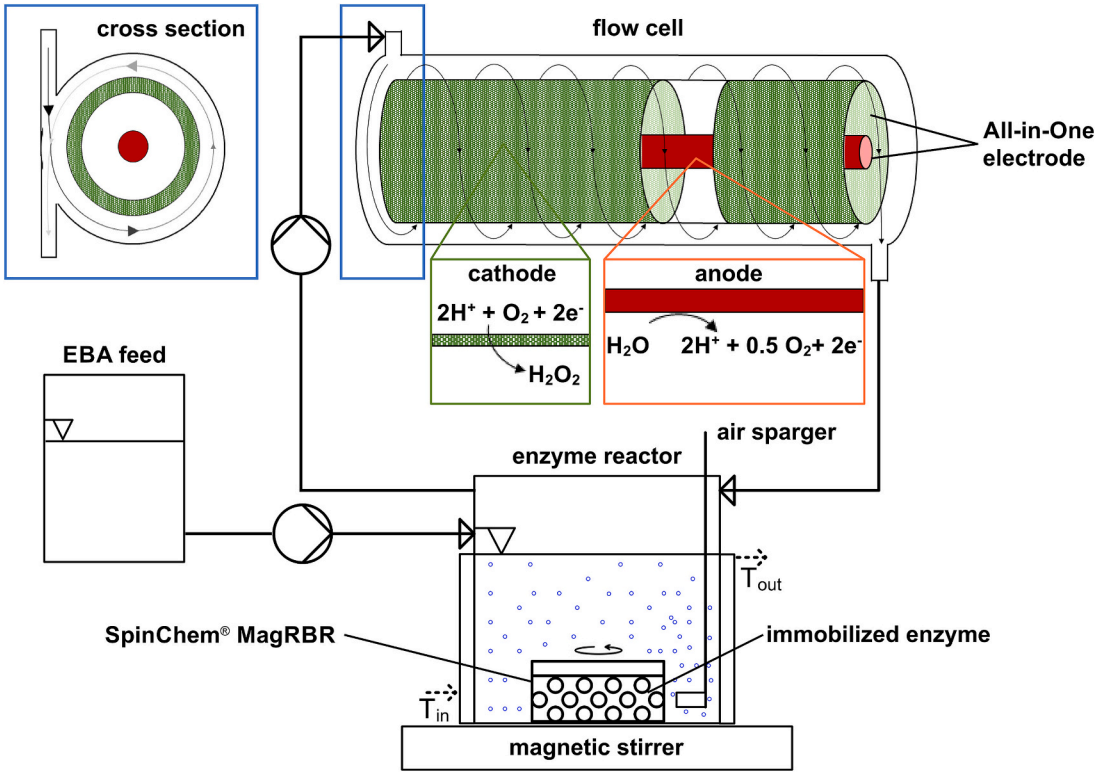

Fig. 1. Illustration of a differentially operated electrochemical flow cell equipped with the All-in-One (AiO) electrode for *in situ* supply of H_2O_2 in a circulation loop reactor. The electrochemical flow cell is operated in a circulation through the enzyme reactor for the electroenzymatic hydroxylation of 4-ethylbenzoic acid (EBA) to 4-(1-hydroxyethyl)benzoic acid (HEBA) catalyzed by immobilized recombinant unspecific peroxygenase from *Agrocybe aegerita* (r*Aae*UPO). The SpinChem® magnetic rotating bed reactor (MagRBR), located inside the enzyme reactor, contains the immobilized r*Aae*UPO.

hydroxylation of 4-ethylbenzoic acid (EBA) to 4-(1-hydroxyethyl)benzoic acid (HEBA) catalyzed by immobilized r*Aae*UPO. r*Aae*UPO is of interest due to its high stability and ability to perform selective oxyfunctionalizations without the need for expensive electron donors like NAD(P)H [47–49]. The immobilization was realized by covalently bound r*Aae*UPO on polymer carriers and contained inside the SpinChem® magnetic rotating bed reactor (MagRBR). Immobilization of enzymes is reported to enhance the operational stability and simplify the separation from the reaction medium [50]. In this case, the separation was further simplified by only removing the SpinChem® MagRBR. The main objective of this research was to establish the proof of concept of the *in situ* electrogeneration of H_2O_2 using the AiO electrode within a flow cell of a circulation loop reactor. The study characterized the *in situ* H_2O_2 electrogeneration and its combination with the hydroxylation reaction catalyzed by immobilized r*Aae*UPO under different current densities. Furthermore, key performance indicators from electroenzymatic processes were determined.

2. Experimental

2.1. Materials

2,2′-Azino-bis(3-ethylbenzothiazoline-6-sulfonic acid) (ABTS) (≥98 %) was purchased from TCI (Eschborn, Germany). HEBA (≥97 %) was purchased from BLD Pharm (China). Zeocin was purchased from InvivoGen (Toulouse, France). Other chemicals were purchased from Carl Roth (Karlsruhe, Germany) or Sigma Aldrich (Steinheim, Germany) in a purity ≥98 %. Carbon felt electrode (area weight: 250 g m^{-2}, thickness: 2.5 mm, surface area (Brunnauer-Emmet-Teller method): 0.4 m^2 g^{-1}) was purchased from SGL Carbon (Sigracell®, Wiesbaden, Germany). Platinized titanium rod electrode (diameter (*d*): 3 mm) was purchased from METAKEM (Usingen, Germany).

2.2. Production of his-tagged rAaeUPO

The *Pichia pastoris* (X33) pre-culture, able to express recombinant protein r*Aae*UPO-PaDa-I-C6His (Prof. Holtmann, Karlsruhe Institute of Technology, Germany), was inoculated overnight in 50 mL buffered complex glycerol (BMGY) medium with 0.0175 mM Zeocin at 200 rpm, 30 °C [51]. The fermentation was conducted in a 1.5 L DASGIP bioreactor system (Eppendorf, Hamburg, Germany) following the protocol described in [51]. Deviations from the original protocol are elaborated in the following. The fermentation was started with a batch phase by inoculating 500 mL basal salt medium (390.3 mM phosphoric acid, 6.8 mM calcium sulfate, 104.4 mM potassium sulfate, 60.5 mM magnesium sulfate heptahydrate, 73.6 mM potassium hydroxide, 434.3 mM glycerol) with the pre-culture. Following the depletion of the initial glycerol, the glycerol fed-batch phase was initiated (feed rate: 13.7–68.4 mmol h^{-1}) and maintained for 24 h. Subsequently, the methanol fed-batch phase was started (feed rate: 0–148.2 mmol h^{-1}) to induce the overexpression of r*Aae*UPO and continued for 120 h. The dissolved oxygen (DO) content and temperature were set at 30 % and 30 °C, respectively. To maintain a constant DO, the stirring rate (400–1200 rpm) and aeration rate (30–60 L h^{-1} ≙ 1 vvm) were regulated by the system. Ammonia solution (13.3 M) was added to maintain the pH at 5. The feeding profile of glycerol and methanol were controlled based on DO levels and set as described in [52]. The biomass was separated *via* centrifugation (Beckmann J2HS, Beckmann Coulter, California, USA) at 5000 rpm for 2 h at 4 °C. The supernatant-containing r*Aae*UPO was sterile-filtered (0.22 μm, DURAPORE, Merck Millipore, Massachusetts, USA) and concentrated by ultrafiltration (10 kDa molecular weight cut off, Minimate TFF Capsule, Pall, New York, USA). The r*Aae*UPO solution was diafiltrated and concentrated in 0.1 M potassium phosphate (KP_i) buffer, pH 7, employing the identical setup utilized for the ultrafiltration step.

2.3. Analytical methods

2.3.1. Quantification of enzyme activity

The ABTS assay was performed in a photometer (Genesys 180, Thermo Scientific, Massachusetts, USA) at 420 nm and at room temperature for 1 min as technical duplicates. The assay consisted of 750 μL 0.1 M Na_2HPO_4/ 0.1 M citric acid buffer pH 4.4, 100 μL 3 mM ABTS, 50 μL 40 mM H_2O_2 and 100 μL r*Aae*UPO sample solution (unknown activity and concentration). The r*Aae*UPO solution was added last to start the reaction. The measurement was started after properly mixing the complete reaction mixture by pipetting up and down 5 times. In the case of the measurement with immobilized r*Aae*UPO, the assay was conducted with 10 mg carrier containing immobilized r*Aae*UPO, 850 μL buffer and mixed with a vortex mixer. The absorbance was monitored for 1 or 10 min. The r*Aae*UPO activity and concentration were calculated as follow [53]:

$$\nu = \frac{slope\ of\ the\ absorbance\ \left[min^{-1}\right] \bullet 10\ (100\ \mu L\ enzyme\ sample\ in\ 1\ mL\ volume)}{36\ \left[mM^{-1}\ cm^{-1}\right] \bullet 1\ cm} \tag{2.1}$$

$$c_{rAaeUPO} = \nu \bullet \frac{(k_m + C_{ABTS})}{k_{cat} \bullet C_{ABTS}} \bullet 1000 \tag{2.2}$$

where ν is the r*Aae*UPO ABTS activity [U_{ABTS} mL^{-1}] (or [U_{ABTS} $g_{carrier}^{-1}$] for immobilized enzyme, with a carrier concentration of 0.25 $g_{carrier}$ mL^{-1} (factor 10 in eq. 2.1 is disregarded for the activity calculation due to the absence of the dilution effect when the immobilized enzyme was used)), C_{ABTS} is the ABTS concentration in the assay [μM], $c_{rAaeUPO}$ is the concentration of r*Aae*UPO [μM], k_m is the Michaelis-Menten parameter (50 μM) [49] and k_{cat} is the catalytic rate constant (546 s^{-1} ≙ 32,760 min^{-1}) [49].

2.3.2. Quantification of H_2O_2 concentration

The assay contained 400 μL sample, 300 μL iodide reagent (0.4 M potassium iodide, 0.05 M NaOH, 10^{-4} M ammonium molybdate) and 300 μL 0.5 M potassium hydrogen phthalate [54]. The mixture was measured directly at 351 nm and at room temperature in technical duplicates. Calibration curves (10 μM to 100 μM) were prepared using diluted H_2O_2 solutions (**Fig. S3**) (lower detection limit of 10 μM).

2.3.3. Quantification of 4-ethylbenzoic acid (EBA) and 4-(1-hydroxyethyl) benzoic acid (HEBA)

The chromatography analysis (Nexera LC-40 HPLC system, Shimadzu, Kyoto, Japan) was carried out at 35 °C using a binary gradient of 0.1 % v/v (13.06 mM) of trifluoroacetic acid (TFA) in H_2O and 0.095 % v/v (12.4 mM) TFA in acetonitrile (ACN) at a flow rate of 0.5 mL min^{-1}. A gradient for ACN was applied as follows: 0 min: 35 %, to 7 min: 80 %, to 9 min: 35 %, to 10 min: 35 %. EBA and HEBA were detected at 237 nm (UV–Vis SPD-40 detector, Shimadzu, Kyoto, Japan) and had retention times of 8.4 min and 4.3 min (Inertsil ODS-P, C18-RP, 5 μm, 100 Å column, GL Science, Japan), respectively (**Fig. S2**). For the sample preparation, a 20 μL sample was mixed with 80 μL 3 % v/v (391.8 mM)

TFA in H_2O, followed by a centrifugation (Biofuge Fresco, Heraeus, Hanau, Germany) at 13,000 rpm and 4 °C for 4 min. The supernatant was transferred to an HPLC-vial and measured as described. Calibration curves (1 mM to 8 mM) were prepared using authentic standards (**Fig. S1**). All measurements were done in technical duplicates.

2.4. rAaeUPO immobilization

The original protocol for the immobilization process provided by the manufacturer of the carrier was used in this study [55]. The epoxy resins (10 g) (Lifetech ECR 8285 [epoxy/ butyl methacrylate]; 400–600 Å, Purolite, King of Prussia, USA) underwent three equilibration cycles in a 1 M KP_i buffer at pH 7, with a resin to buffer ratio of 1:1 w/v, using an overhead shaker at 80 rpm and 22 °C for 10 min each time. Separately, the r*Aae*UPO was diluted, also with 1 M KP_i buffer pH 7, to reach a final activity of 20 U_{ABTS} mL^{-1} in a total volume of 40 mL. The epoxy resin and the r*Aae*UPO were combined in a 50 mL falcon tube to achieve a final resin to buffer ratio of 1:4 w/v. The mixture was incubated on an overhead shaker at 80 rpm and 22 °C for 18 h, followed by static incubation at the same condition for an additional 20 h. Washing steps were conducted three times using 40 mL of 0.01 M KP_i buffer pH 7, following the equilibration cycle protocol. The resulting immobilized enzyme was stored in a 0.1 M KP_i buffer pH 7 and kept at 4 °C. The activity and concentration of the immobilized enzyme used for calculations in this study were determined based on the measured activity and their corresponding concentrations, as described in section *2.3.1*.

2.5. Electrochemical setup

Electrochemical and electroenzymatic experiments were conducted in a circulation loop reactor consisting of electrochemical flow cell (made out of a polyether ether ketone (PEEK) material) and an enzyme reactor with a total working volume of 50 mL. The flow cell has an inner diameter of 12.4 mm and a length (*l*) of 65 mm, with a volume of 7.8 mL without the AiO electrode installed or 1.7 mL with the AiO electrode installed (Fig. 2). To induce a circular flow inside the flow cell, inlet and outlet (*d*: 1.5 mm) flows were tangentially directed into and out of the flow cell. The AiO electrode (*l* within the flow cell: 62 mm, *d* within the flow cell: 12 mm, M20x1.5 thread to connect the AiO electrode into the flow cell) was fitted with the carbon felt as the working electrode (cathode) (*A*: 8.3 cm^2) and integrated into the flow cell (Fig. 2). A platinized titanium rod (*A*: 4.24 cm^2) was used as the counter electrode (anode) and located inside the AiO electrode scaffold. A perforated cylindrical separator with an outer diameter of 9 mm and thickness of 1 mm was used to separate the cathode and anode (Fig. 2). The AiO electrode was fixed and not operated as a rotating electrode. Water electrolysis takes place at the anode generating O_2 and H^+ molecules *in situ*. These molecules diffuse from the anode towards the cathode, where O_2 is reduced at the surface of the cathode to react with H^+ to H_2O_2, which subsequently used as co-substrate for the enzymatic hydroxylation inside the SpinChem® MagRBR. The SpinChem® MagRBR (*d*: 19.5 mm, *h*: 13.7 mm, SpinChem AB, Umeå, Sweden) contained the immobilized enzyme and was located inside the enzyme reactor (Fig. 1).

2.6. Electroenzymatic experiments

Experiments were operated either as batch or fed-batch (EBA feed). Unless otherwise stated, the reaction medium contained 50 mL 0.1 M KP_i pH 7, 8 mM EBA and 0.8 g (40 nM, 1.4 U_{ABTS} $g^{-1}_{carrier}$) carrier containing immobilized r*Aae*UPO contained inside the SpinChem® MagRBR. The enzyme reactor was sparged with air at 4 vvm using a porous sintered frit sparger [56] (microbubble generator, *d*: 13 mm, *l*: 25 mm) having an average pore diameter of 5 µm. A circulation flow rate of 24 mL min^{-1} was pumped through the flow cell (resulting residence

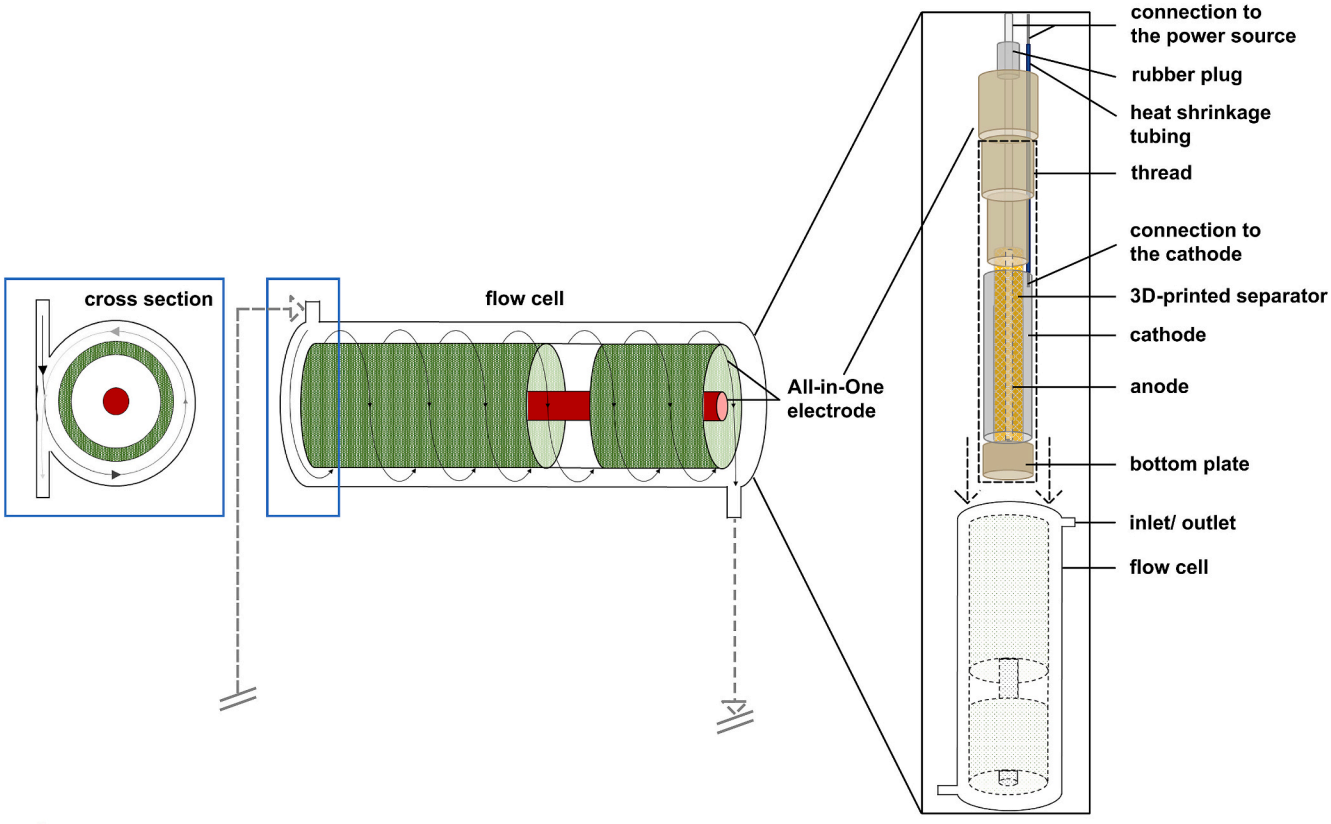

Fig. 2. Illustration of the electrochemical flow cell equipped with the All-in-One (AiO) electrode for the *in situ* electrochemical generation of H_2O_2. Dimensions, volumes and technical descriptions are delineated in the text.

time in the flow cell (τ_{FC}): 0.07 min) and the enzyme reactor (resulting residence time in the enzyme reactor (τ_{ER}): 2.01 min). In the case of fed-batch operation, 200 mM EBA solution was fed at a rate of either 0.008, 0.012 or 0.016 mmol h^{-1} (40, 60 or 80 µL h^{-1}). The EBA feed was started after 90 min. The SpinChem® MagRBR speed was set to 1000 rpm. Galvanostatic experiments were performed at a current density between 0.61 mA cm^{-2} and 3.64 mA cm^{-2} (Keithley 2231a-30-3 DC power supply, Tektronix, Oregon, USA). Samples for the measurement of EBA, HEBA, H_2O_2 concentration, and r*Aae*UPO activity were taken periodically from the enzyme reactor. Each experiment was conducted at 22 ± 1 °C and stopped after 24 h, and performed in duplicates.

The total turnover number (TTN) is defined as the quotient of the final product concentration once the enzyme was deactivated ($C_{HEBA,t=end}$) and the applied enzyme concentration ($C_{rAaeUPO}$) (equation (eq.) 2.3). Meanwhile, the turnover number (TON) is described as the quotient of the product concentration at a specific time (at 60 min) before the enzyme was deactivated ($C_{HEBA,t=60\ min}$) and the applied enzyme concentration (eq. 2.4). The turnover frequency (TOF) refers to the TON per unit time and were calculated from the initial part (≤15 % conversion, 60 min) of the experiment where the product formation was linear (eq. 2.5).

$$TTN = \frac{C_{HEBA,t=end}\ [mol]}{C_{rAaeUPO}\ [mol]} \tag{2.3}$$

$$TON = \frac{C_{HEBA,t=60\ min}\ [mol]}{C_{rAaeUPO}\ [mol]} \tag{2.4}$$

$$TOF = \frac{TON}{3600\ s} \tag{2.5}$$

The H_2O_2 productivity was determined at current densities between 0.61 mA cm^{-2} and 3.64 mA cm^{-2}, within the same setup under abiotic condition and performed in duplicates. The Faradaic efficiency (F.E.) describes how much energy is consumed for the formation of H_2O_2 or the formation of side products, and was determined as follow [35].

$$F.E. = \frac{n \bullet F \bullet C_{H_2O_2} \bullet V}{Q\left(\int_{t=0}^{t=t} I(constant)dt\right)} \tag{2.6}$$

where n is the number of transferred electron (2), F is the Faraday constant (96,500 C mol^{-1}), $C_{H_2O_2}$ is the accumulated H_2O_2 concentration in the medium [M], V is the volume of the reaction medium [L] and Q is the total charge [C], which was calculated by integrating the applied current over time.

3. Results and discussion

In order to validate the feasibility of *in situ* electrogeneration of H_2O_2

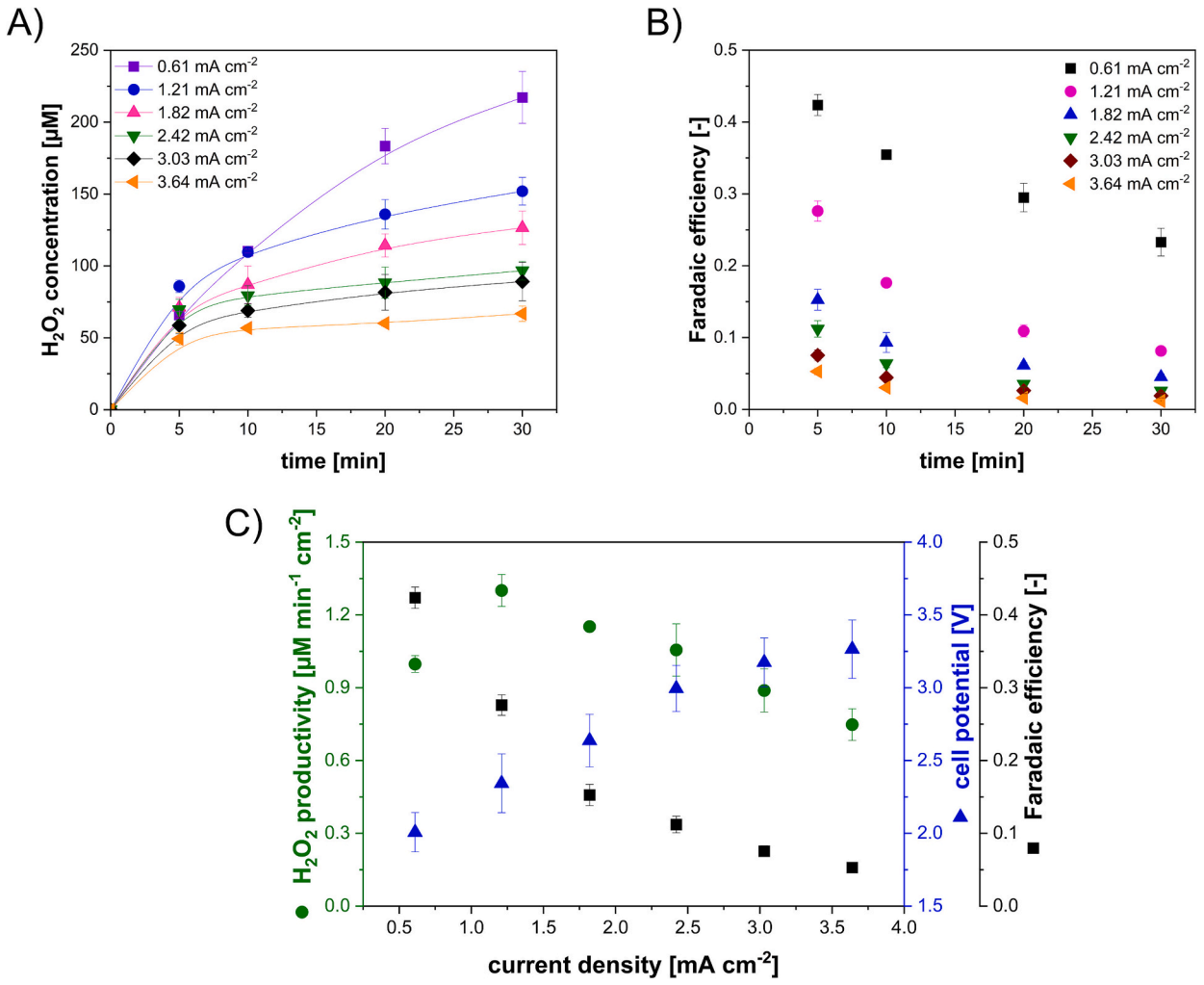

Fig. 3. A) H_2O_2 concentration as a function of time at different current densities. B) Faradaic efficiency (F.E.) as a function of time at different current densities. C) Specific H_2O_2 productivity, resulting cell potential and F.E. (t: 5 min) as a function of current density. Conditions: carbon felt working electrode (8.3 cm^2), platinized titanium counter electrode (4.24 cm^2), 50 mL 0.1 M KP_i pH 7, at 22 ± 1 °C, 1000 rpm, circulation flow rate: 24 mL min^{-1} (resulting τ_{FC}: 0.07 min and τ_{ER}: 2.01 min) and 4 vvm. Duplicates were performed. Depicted lines serve as a visual aid.

using the AiO electrode within a flow reactor technology, it was first necessary to characterize the productivity of H_2O_2 in dependence of current density, aeration rate and liquid residence time. Subsequently, the *in situ* H_2O_2 generation within the flow cell was combined with the enzymatic hydroxylation reaction under batch and fed-batch operation modes catalyzed by the immobilized r*Aae*UPO to establish a BES.

3.1. *In situ electrogeneration of H_2O_2 within the electrochemical flow cell system*

The AiO electrode, equipped with a carbon felt cathode, was integrated into a flow cell and applied in a circulation loop of an enzyme reactor, as illustrated in Fig. 1. Prior to starting the electroenzymatic hydroxylation reaction, a characterization study was done to evaluate the AiO electrode's ability to generate H_2O_2 *in situ*, especially, within a flow cell of a circulation loop reactor. This assessment was conducted in an abiotic environment, without the addition of biocatalyst and substrate EBA. Fig. 3 illustrates the specific productivity, the Faradaic efficiency (F.E.), and the resulting cell potential in relation to current density.

As depicted in Fig. 3**. A**, the H_2O_2 concentration exhibits a gradual increase over time across all applied current densities and eventually reaching a maximum value of approximately 217 μM after 30 min at 0.61 mA cm^{-2}. Although an increasing trend is still observed between 20 and 30 min, the H_2O_2 generation rate had already declined, indicating that the H_2O_2 accumulation is approaching an asymptotic trend. This steady-state condition arises when the generation rate of H_2O_2 is equivalent to the rate of: (1) its reduction at the cathode (eq. 3.1), which occurs due to the accumulation of H_2O_2 at the working electrode, or its competing reactions such as (2) oxidation at the anode (eq. 3.2), (3) hydrogen evolution reaction (eq. 3.3) or (4) full reduction of oxygen to water (eq. 3.4) *via* the four-electron reduction mechanism [57,58]. Extending the reaction time would not necessarily lead to a significant increase in the accumulation of H_2O_2 concentration.

$$H_2O_2 + 2H^+ + 2e^- \rightarrow 2H_2O \quad (3.1)$$

$$H_2O_2 \rightarrow 2H^+ + O_2 + 2e^- \quad (3.2)$$

$$2H^+ + 2e^- \rightarrow H_2 \quad (3.3)$$

$$O_2 + 4H^+ + 4e^- \rightarrow 2H_2O \quad (3.4)$$

An increase in the applied current density from 0.61 mA cm^{-2} to 1.21 mA cm^{-2} leads to an increase in the productivity of H_2O_2 from 0.99 μM min^{-1} cm^{-2} to 1.30 μM min^{-1} cm^{-2} (Fig. 3**. C**). However, a further increase of the applied current density above 1.21 mA cm^{-2} leads to a decrease of the H_2O_2 productivity. This trend can also be observed for the accumulation of the H_2O_2 concentration, as already shown in Fig. 3**. A**. The decrease in both productivity and accumulation of H_2O_2 with increasing applied current can be explained by the increasing rate of competing reactions mentioned earlier. Prior studies have also reported a similar observation, where the rate of competing reactions increased with an increase in the applied current density [54,59]. Peralta et al., even reported an increased rate of competing reactions already at a current density of 0.38 mA cm^{-2} [60]. In the meantime, the cell potential shows a linear increase from 2.0 V to 3.3 V as the current density is increased.

The F.E, depicted in Fig. 3**. B**, is decreasing over time, for all applied current density. This behavior occurs because in the beginning of the experiment, the concentration of H_2O_2 in the medium and at the electrode was zero. Thus, the decomposition rate of H_2O_2 was equally zero. As the electrolysis progresses, the H_2O_2 concentration in the medium and at the electrode increases, and, at the same time, the rate of its decomposition and side reactions become more pronounce and relevant. Of particular significance are the cathodic reduction of H_2O_2 and the complete reduction of oxygen to water. In other studies, comparable F.Es. from electrochemical systems equipped with a carbon based electrode are reported, which ranges between 0.18 and 0.57 [25,60,61]. Considering the achieved H_2O_2 productivity and the F.E. (Fig. 3**. C**), the optimal electrochemical operation window would be between 0.61 and 1.21 mA cm^{-2}. This interval represents the compromise point between the highest H_2O_2 productivity and the highest F.E. within the investigated range of current density. The specific electrode area in this study corresponds to 0.17 cm^{-1}, which is comparable to electrochemical cells such as chloralkali cells and is lower than fluidized-bed cells or porous flow through cells, which typically ranges between 10 and 100 cm^{-1} [62].

Given that the H_2O_2 generation by the AiO electrode occurs within the flow cell, the oxygen availability may pose a limiting factor that could affect the H_2O_2 productivity. Since the *in situ* oxygen generation takes place at the anode, the lack of rigorous stirring in a flow cell could impact the oxygen distribution and mass transfer towards the cathode. Furthermore, it is important to note the electron balance during the process: for every H_2O_2 molecule generated at the cathode ($O_2 + 2H^+ + 2e^- \rightarrow H_2O_2$), only half an oxygen molecule is generated at the anode ($H_2O \rightarrow 2H^+ + \frac{1}{2}O_2 + 2e^-$). This imbalance may exacerbate the oxygen limitation. To address these subjects, the *in situ* H_2O_2 electrogeneration was tested at 1.21 mA cm^{-2}, while varying the aeration rate inside the enzyme reactor and the liquid residence time inside the flow cell (τ_{FC}), by varying the circulation flow rate. In this way, the influence of these parameter on the productivity of the H_2O_2 was determined.

In the previous experiments, the enzyme reactor was sparged with an aeration rate of 4 vvm to supply additional oxygen to the cathode for the electrosynthesis of H_2O_2. Increasing the aeration rate by a factor of three did not further increase the initial productivity (see **Fig. S5** for the full data set) and the accumulation of H_2O_2 concentration. However, completely eliminating the aeration in the enzyme reactor significantly reduced both productivity, from 1.30 μM min^{-1} cm^{-2} to 0.53 μM min^{-1} cm^{-2}, and H_2O_2 accumulation after 30 min, from 152 μM to 69 μM (Fig. 4**. A** & **C**). This difference can be attributed to the stoichiometry of the electrochemical reactions. Since only half an oxygen molecule is generated at the anode, while a full oxygen molecule is required at the cathode for H_2O_2 formation, the anode reaction must occur twice to generate one oxygen molecule. Introducing additional aeration compensates for this oxygen deficit, preventing oxygen limitation at the cathode and enabling unrestricted H_2O_2 formation. Consequently, with sufficient oxygen supply, the productivity doubled, aligning with theoretical expectation. It can be concluded, that under chosen experiment conditions the oxygen availability is one of the limiting factors. Thus, it is beneficial to introduce an aeration into the enzyme reactor to supply additional oxygen molecules to the cathode for the generation of H_2O_2. The concern regarding the oxygen availability, especially due to its solubility and diffusivity towards the electrode, during the electrosynthesis of H_2O_2 was also expressed in former studies [63,64]. In a conventional stirred tank reactor with 3D carbon-based electrode, this limitation is normally being resolved by sparging air or pure oxygen and rigorous mixing [65,66]. The flow rate of pure oxygen utilized in these studies ranges from 1.3 to 7 vvm [64,66], while this study employs an aeration rate of 4 vvm of air. The absence of an increase in the H_2O_2 productivity following an increase in the aeration rate by a factor of three in this case can be attributed to two factors: (1) the maximum oxygen solubility in the enzyme reactor (0.25 mM at room temperature and atmospheric pressure [26]) could have been reached, and (2) oxygen mass transport limitation from the enzyme reactor towards the cathode in the flow cell has been encountered, given that the aeration and the cathodic reduction of oxygen are separated. Therefore, not only the current density and the aeration rate are of the essence for the H_2O_2 electrogeneration, but also the τ_{FC} (determined by the circulation flow rate).

As previously mentioned, although the aeration rate inside the enzyme reactor was increased, the oxygen molecules had to diffuse to-

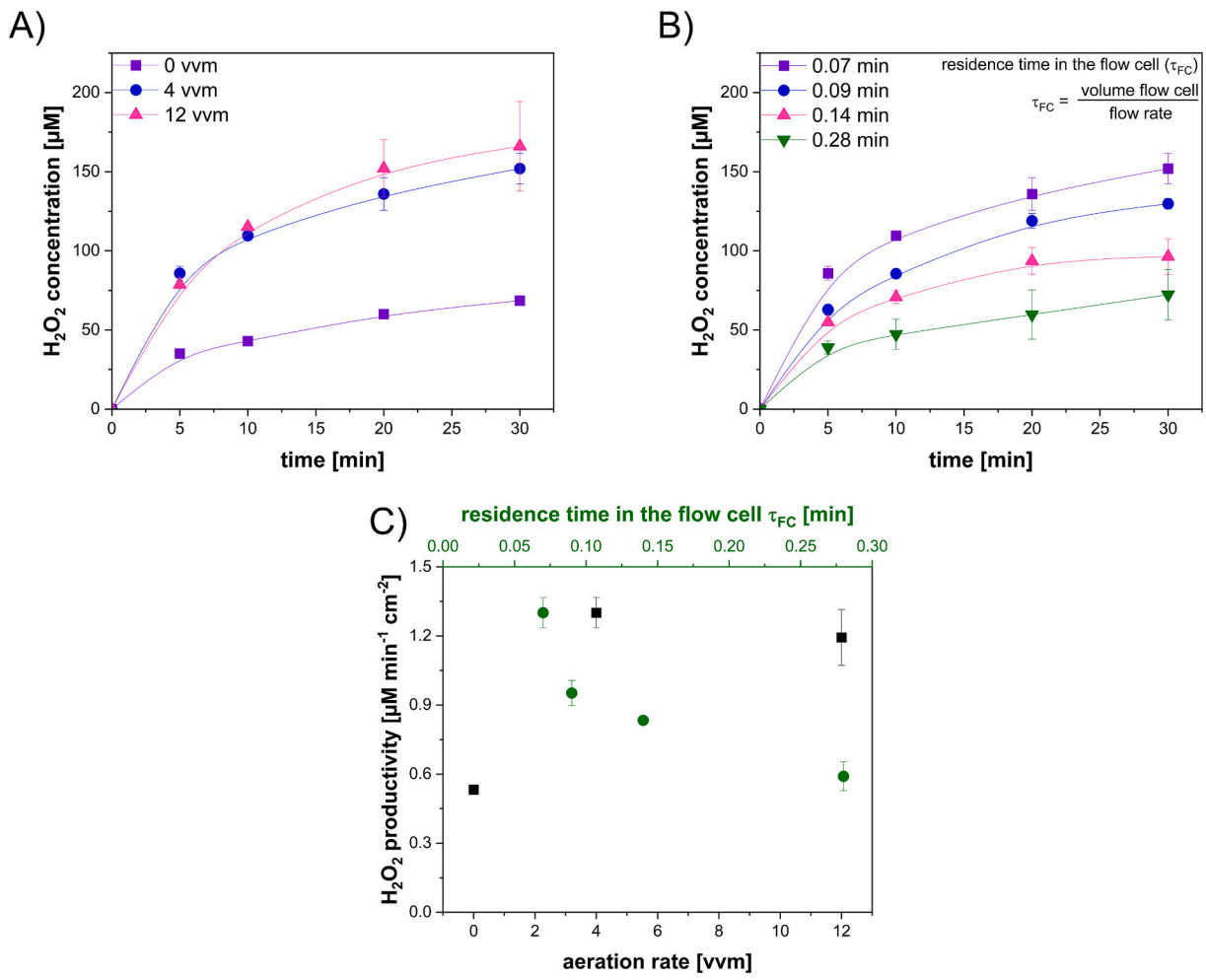

Fig. 4. A) H_2O_2 concentration as a function of time at different aeration rates. B) H_2O_2 concentration as a function of time at different residence times in the flow cell (τ_{FC}). τ_{FC} of 0.28, 0.14, 0.09 and 0.07 min correspond to circulation flow rates of 6, 12, 18 and 24 mL min^{-1}, respectively. C) Specific H_2O_2 productivity as a function of aeration rate and as a function of τ_{FC} (independent from each other). Conditions: carbon felt working electrode (8.3 cm^2), platinized titanium counter electrode (4.24 cm^2), 1.21 mA cm^{-2}, 50 mL 0.1 M KP_i pH 7, at 22 ± 1 °C, 1000 rpm, circulation flow rate: 24 mL min^{-1} (resulting τ_{FC}: 0.07 min and τ_{ER}: 2.01 min) (if the τ_{FC} was not varied) and 4 vvm (if the aeration rate was not varied). Duplicates were performed. Depicted lines serve as a visual aid.

wards the cathode inside the flow cell. The oxygen mass transfer towards the cathode in this instance is defined by the circulation flow rate, which carries the dissolved oxygen from the enzyme reactor to the cathode in the flow cell. By adjusting the circulation flow rate through the flow cell, thus also the residence time in the flow cell (τ_{FC}), the mass transfer of the dissolved oxygen to the cathode can be influenced. As shown in Fig. 4. **B** & **C**, the accumulation and the productivity of H_2O_2 is increasing with a decrease in the τ_{FC} (increase in the circulation flow rate), at the same aeration rate. By decreasing the τ_{FC} from 0.28 min to 0.07 min (increasing the flow rate from 6 mL min^{-1} to 24 mL min^{-1}), the productivity and the accumulation of H_2O_2 after 30 min increase from 0.59 µM min^{-1} cm^{-2} to 1.30 µM min^{-1} cm^{-2} and from 72.3 µM to 151.9 µM, respectively. Nevertheless, the increase in the productivity and the accumulation cannot be attributed solely due to the increase in the oxygen mass transfer to the cathode, but also due to a faster desorption of formed H_2O_2 from the cathode surface owing to an increase of the flow rate. The Reynolds (Re) number at the highest flow rate tested in this study is 84.73 (Re <2300), meaning that the flow is still in the laminar region (eq. S1.1 and eq. S1.2). Because of a faster H_2O_2 desorption from the electrode surface, further redox reactions of H_2O_2 are minimized, leading to a higher H_2O_2 accumulation and measured productivity in the medium. Correspondingly, the F.E. after 30 min increased from 0.04 at a τ_{FC} of 0.28 min (circulation flow rate: 6 mL min^{-1}) to 0.08 at a τ_{FC} of 0.07 min (circulation flow rate: 24 mL min^{-1}). Additionally, the decrease of the circulation flow rate (increase in the τ_{FC}) leads to a potentially thicker electrochemical double layer at the interface of the cathode and the medium. Thus, increasing the resistance of the electron transfer, which is reflected by the increase in the resulting cell potential from 2.34 V to 2.71 V, at the same current density of 1.21 mA cm^{-2}. In return, the increase of the resulting cell potential favors the full reduction of oxygen and reduction of H_2O_2 to water. The influence of the flow rate and the τ_{FC} on the H_2O_2 productivity and its accumulation at a lower current density, such as at 0.61 mA cm^{-2} (**Fig. S6**), is less apparent due to the fact that at lower current density, the mass transport phenomena is not the limiting factor for the H_2O_2 productivity, but rather controlled by the applied current (current determines the H_2O_2 productivity). At the same time, the rate of competing reactions like further redox reaction of formed H_2O_2, full reduction of oxygen to water and hydrogen evolution reaction is less prominent. In this instance, the H_2O_2 productivity and its accumulation is increased by a factor of 1.5 by decreasing the τ_{FC} from 0.28 min to 0.07 min (increasing the circulation flow rate from 6 mL min^{-1} to 24 mL min^{-1}). As illustrated in Fig. 4. **C**, the maximum obtained specific H_2O_2 productivity indicates that the *in situ* electrogeneration of H_2O_2 within this setup is optimal when an aeration rate of 4 vvm and a τ_{FC} of 0.07 min are employed.

An experiment with a flow rate exceeding 24 mL min^{-1} (τ_{FC}: 0.07 min) was not conducted due to the pump reaching its maximum flow rate. One potential strategy for further enhancing the electrochemical

productivity of H_2O_2 is the application of high pressure within the system. This approach has been demonstrated to enhance the solubility of oxygen and its mass transfer, thereby also increasing the productivity of H_2O_2 [59]. Overall, the H_2O_2 productivity generated by the AiO electrode in a flow cell obtained in this study is comparable to productivities reported in the literature. The reported values range from 0.03 to 2.1 μM min^{-1} cm^{-2} [54,60,67,68] and the AiO electrode system employed in a stirred tank reactor reported a productivity of 0.87 μM min^{-1} cm^{-2} [44]. Following the characterization study of *in situ* electrosynthesis of H_2O_2, the *in situ* supply of H_2O_2 was combined with the enzymatic hydroxylation reaction to establish a BES.

3.2. Electroenzymatic hydroxylation of 4-ethylbenzoic acid (EBA)

After the characterization of the H_2O_2 electrosynthesis in a flow cell of the circulation loop reactor, the electrochemical and the biocatalytic systems were combined to form a BES for the hydroxylation of EBA to HEBA, catalyzed by immobilized r*Aae*UPO. EBA was selected as the model substrate over benzene or ethylbenzene due to its non-volatility and high solubility in aqueous solution [69]. The solubility of EBA in a 0.1 M KP_i buffer pH 7 is approximately 10 mM [69], whereas the solubility of benzene and ethylbenzene in water is approximately 20 mM [70] and 1.6 mM [71], respectively. Additionally, the application of EBA eliminates the potential formation of by-products or subsequent reactions that could affect the reaction selectivity, a concern that arises in the application of benzene and ethylbenzene [23,72].

Immobilized biocatalysts are often used both in a lab or in an industrial application [50]. General advantages of enzyme immobilization are, among others, increase of enzyme operational stability and ease of recovery from the reaction medium [73]. In this specific case, a direct immobilization of r*Aae*UPO on the surface of the electrode was an attractive option, because, then, the electrode does not only supply the cosubstrate H_2O_2, but also works as a carrier for the enzyme. Furthermore, this approach would increase the proximity between the enzyme and the cosubstrate, potentially increasing the efficiency of the biocatalytic reaction. However, a direct immobilization of r*Aae*UPO on the electrode surface led to a faster deactivation (**Fig. S7**). A faster deactivation could be attributed to the following factors: (1) the r*Aae*UPO reacted directly with the formed H_2O_2 and radicals such as superoxide and hydroxyl radical on the electrode, and (2) a possible diffusion limitation of the EBA into the pores, where the r*Aae*UPO was immobilized, prompted further reactions only between r*Aae*UPO and H_2O_2, thus, leading to a catalase malfunction reaction [74]. In this contribution, an alternative immobilization strategy was employed, involving the covalent binding of r*Aae*UPO onto an epoxy resins carrier. Epoxy-activated resins are regarded as optimal matrices for enzyme immobilization due to their capacity for providing multipoint covalent binding between the enzyme and the resin carrier [55]. The carrier was then placed within the SpinChem® MagRBR, which was positioned inside the enzyme reactor of the circulation loop reactor (Fig. 1).

The immobilization of r*Aae*UPO on the Lifetech ECR 8285 epoxy resins carrier resulted in an immobilization yield of 85.2 % and an activity yield of 1.75 %, with a measured activity of 1.4 ± 0.3 U_{ABTS} $g^{-1}_{carrier}$. The calculated activity loss, derived from residual r*Aae*UPO activities in the supernatant following the immobilization process and washing steps, was 2.95 U_{ABTS} mL^{-1} (**Table S1**). The theoretical activity of immobilized r*Aae*UPO on the carrier based on the immobilization yield was 68.2 U_{ABTS} $g^{-1}_{carrier}$. In this study, the immobilization efficiency was calculated by dividing the measured immobilized enzyme activity by the theoretical immobilized enzyme activity, resulting in an efficiency of 2.05 %. In comparison with the values reported in the literature, the immobilization yield and activity yield obtained in this study are approximately 1.57 and 3.97 times higher, respectively [75]. However, the specific activity is approximately 70 % lower. A low activity yield, specific activity and immobilization efficiency despite a high immobilization yield could indicate the presence of steric hindrance and mass transport limitation during the activity assay in the photometer. This is despite the fact that the reaction mixture and the immobilized enzyme were mixed with a vortex mixer prior to the measurement. Furthermore, despite the carrier underwent three washing cycles after the immobilization step, with a maximum of 2.95 U_{ABTS} mL^{-1} removed, there remained the possibility of multilayer adsorption of the enzyme on the carrier.

Electroenzymatic experiments were performed for 24 h at various current densities between 0.61 mA cm^{-2} and 3.64 mA cm^{-2} in a batch operation mode. The reaction medium consisted of 8 mM EBA and 0.8 g of carrier containing immobilized r*Aae*UPO, contained within the SpinChem® MagRBR. H_2O_2 was generated *in situ* by the AiO electrode inside the flow cell. The dissolved H_2O_2 was then circulated through the enzyme reactor, where the hydroxylation occurred. The concentrations of EBA, HEBA and H_2O_2 during the experiments were measured and are depicted in Fig. 5.

To monitor the potential of enzyme leaching, samples were withdrawn from the medium at a specific frequency in order to measure the r*Aae*UPO activity *via* the ABTS assay. The ABTS assays indicated that r*Aae*UPO activity was not detected in the reaction medium supernatant, suggesting that the immobilized r*Aae*UPO was not detached from the carrier. As illustrated in Fig. 5, the productivity and the accumulation of H_2O_2 during the electroenzymatic hydroxylation reaction are dependent on the current density. At lower current density such as 0.61 mA cm^{-2} (Fig. 5**. A**), the H_2O_2 productivity was lower. However, the H_2O_2 concentration was gradually increasing over time and accumulated to 0.7 mM after 7 h, and higher than 1.5 mM after 24 h. In contrast, at higher current density such as 1.82 mA cm^{-2} and 2.42 mA cm^{-2} (Fig. 5**. C** & **D**), the H_2O_2 productivity was comparably faster and the H_2O_2 concentration accumulated to a concentration around 1.1 mM after 7 h. Albeit, this concentration did not significantly increase after 24 h. It is important to note that in Fig. 5**. C** and **D**, the final H_2O_2 concentrations are lower than the preceding measurement points. The discrepancy was caused by the inlet tubing of the flow cell inside the enzyme reactor being drawn into the vortex above the SpinChem® MagRBR. This resulted in a mixture of air and liquid being sucked into the flow cell, forming a slug flow that impeded the H_2O_2 generation due to the disruption of the continuous liquid flow by gas bubbles at the cathode. Simultaneously, the existing H_2O_2 in the enzyme reactor was consumed during the hydroxylation process, further contributing to the observed reduction in the concentration. At the highest tested current density of 3.64 mA cm^{-2} (Fig. 5**. F**), the productivity of H_2O_2 decreased, with the H_2O_2 concentration fluctuating around 0.3 mM. As previously discussed, the observed decline in both H_2O_2 productivity and its accumulation can be attributed to the increasing rate of the H_2O_2 decomposition and competing reactions. After 24 h and for each experiment, the immobilized r*Aae*UPO was deactivated. This was confirmed by the ABTS assay, which was performed using 10 mg of the carrier taken from within the SpinChem® MagRBR. The relevant performance indicators from the electroenzymatic experiments such as TTN, TOF, catalytic productivity and final HEBA concentration are summarized in Table 1.

Within an electroenzymatic system, particularly utilizing peroxygenases and peroxidases, the productivity and the accumulation of H_2O_2 inside the medium determine not only the biocatalytic productivity but also the enzyme stability. A higher and faster accumulation of H_2O_2 within the medium will result in a higher degree of enzyme saturation with the H_2O_2. This, in turn, will result in a higher biocatalytic rate ($K_{M,H2O2}$: 0.79–1.8 mM [37,49,74]) and TOF, reaching a maximum of 8.34 $\pm$ 0.14 s^{-1}. Simultaneously, the higher the accumulation of H_2O_2 and the catalytic rate, the higher the probability of r*Aae*UPO undergoing an unproductive catalytic cycle, such as a catalase reaction. Even a catalase malfunction reaction occurs more frequently, which leads to an enzyme deactivation. The aforementioned reaction and its mechanism have been previously proposed [74]. The catalase malfunction reaction can be attributed to the subsequent reactions between the intermediate compound I, which is formed after the resting state of r*Aae*UPO binds with

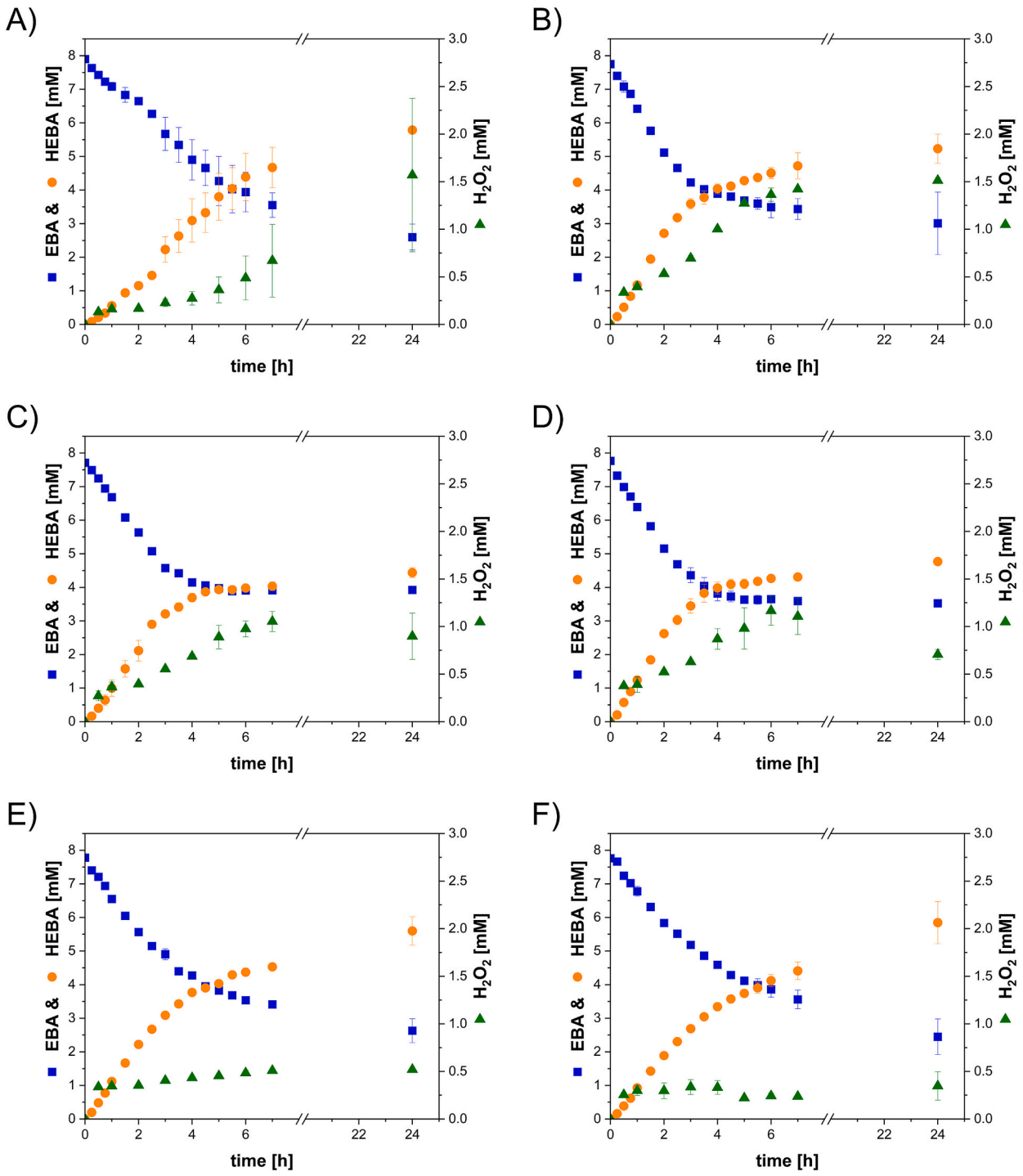

Fig. 5. Hydroxylation of EBA catalyzed by immobilized r*Aae*UPO in a circulation loop reactor equipped with the All-in-One electrode for *in situ* H_2O_2 generation at A) 0.61 mA cm^{-2}, B) 1.21 mA cm^{-2}, C) 1.82 mA cm^{-2}, D) 2.42 mA cm^{-2}, E) 3.03 mA cm^{-2} and F) 3.64 mA cm^{-2}. Conditions: 50 mL 0.1 M KP_i pH 7, 8 mM EBA, 0.8 g carrier (40 nM r*Aae*UPO), 1000 rpm, circulation flow rate: 24 mL min^{-1} (resulting τ_{FC}: 0.07 and τ_{ER}: 2.01 min), 4 vvm and at 22 ± 1 °C. EBA: 4-ethylbenzoic acid, HEBA: 4-(1-hydroxyethyl)benzoic acid. Duplicates were performed.

the first H_2O_2 molecule, and a further H_2O_2 molecule instead of with the substrate EBA. The reaction of the intermediate compound I with the second H_2O_2 molecule yields the intermediate compound II. Subsequently, compound II is susceptible to further reactions with additional H_2O_2, resulting in the formation of compound III. The formation and the presence of compound III would ultimately result in the heme-bleaching of r*Aae*UPO. This is because if the compound III were to be exposed to additional H_2O_2, it would form free radicals, which would cause heme-destruction and result in the irreversible deactivation [37,74]. Additionally, the deactivation due to the degradation of heme is inevitable and correlated directly with the product formation [29]. The catalase and catalase malfunction reactions are intensified at lower concentrations of EBA, given that the reported K_M value of EBA, which is 2.3 mM [37], is higher than the K_M value of H_2O_2. Under these conditions, applying or achieving during the course of a reaction EBA concentrations close or below its K_M value not only diminishes the catalytic rate but also promotes the catalase malfunction reaction due to the continuous presence of H_2O_2. Consequently, this leads to an accelerated

Table 1
Summary of total turnover number (TTN), turnover frequency (TOF), catalytic productivity and final concentration of HEBA determined from electroenzymatic experiments in the circulation loop reactor equipped with the All-in-One electrode at various current densities.

current density [mA cm^{-2}]	catalytic productivity [mM h^{-1}]	final HEBA concentration [mM]	TOF [s^{-1}]	TTN [mol mol^{-1}]
0.61	0.56 ± 0.07	5.79 ± 0.03	3.77 ± 0.45	$1.40 \cdot 10^5$ ± 840
1.21	1.18 ± 0.02	5.23 ± 0.43	7.91 ± 0.07	$1.26 \cdot 10^5$ ± 10,458
1.82	1.24 ± 0.11	4.44 ± 0.15	6.74 ± 1.64	$1.07 \cdot 10^5$ ± 3,623
2.42	1.24 ± 0.02	4.77 ± 0.09	8.34 ± 0.14	$1.15 \cdot 10^5$ ± 2,143
3.03	1.12 ± 0.02	5.60 ± 0.42	7.53 ± 0.15	$1.35 \cdot 10^5$ ± 10,194
3.64	0.92 ± 0.01	5.85 ± 0.63	6.23 ± 0.04	$1.41 \cdot 10^5$ ± 15,225

Conditions: 50 mL 0.1 M KP_i pH 7, 8 mM EBA, 0.8 g carrier (40 nM r*Aae*UPO), 1000 rpm, circulation flow rate: 24 mL min^{-1} (resulting τ_{FC}: 0.07 and τ_{ER}: 2.01 min), 4 vvm and at 22 ± 1 °C. Duplicates were performed.

r*Aae*UPO deactivation as the H_2O_2 productivity and its accumulation increase. As a result, the final concentration of HEBA is reduced. This phenomenon is evident in the observation that at the highest TOF of 8.34 ± 0.14 s^{-1}, one of the lowest final HEBA concentration (4.77 ± 0.09 mM) and also one of the lowest TTN of $1.15 \cdot 10^5$ ± 2,143 mol mol^{-1} are obtained (Table 1). Conversely, at the lowest TOF of 3.77 ± 0.45 s^{-1}, one of the highest TTN values is obtained, corresponding to $1.40 \cdot 10^5$ ± 840 mol mol^{-1}. Slight variations in H_2O_2 accumulation in the medium during the reaction and sampling error could explain the deviation of measured substrate and product, thus also deviations in both TOF and TTN. Additional control experiments, in which the substrate or product were circulated for 7 h through the circulation loop reactor, revealed no substantial adsorption of substrate or product on the electrode surface, tubing or PEEK material (**Fig. S4**). Furthermore, the mass transport of the liquid into and out of the SpinChem® MagRBR was impeded by the carrier loading and the surface roughness, leading to an incomplete utilization of the immobilized enzyme. This was confirmed by reducing the carrier loading by 50 % (0.4 g) (**Fig. S8**). Under the same reaction conditions at 1.21 mA cm^{-2}, the catalytic rate achieved with the reduced carrier was 0.79 mM h^{-1}, which corresponded to 67 % of the rate observed with full carrier loading (0.8 g). This rate exceeded the expected value of 0.59 mM h^{-1}, suggesting that the enzyme's activity was not fully utilized in the higher carrier loading scenario.

As discussed in section *3.1*, in addition to the current density, the residence time in the flow cell (τ_{FC}) (determined by the circulation flow rate) could affect the productivity and the accumulation of H_2O_2 during the experiment. Therefore, after the initial establishment of a BES using the integrated flow cell in a circulation loop reactor, the influence of the residence time on the electroenzymatic hydroxylation was also investigated.

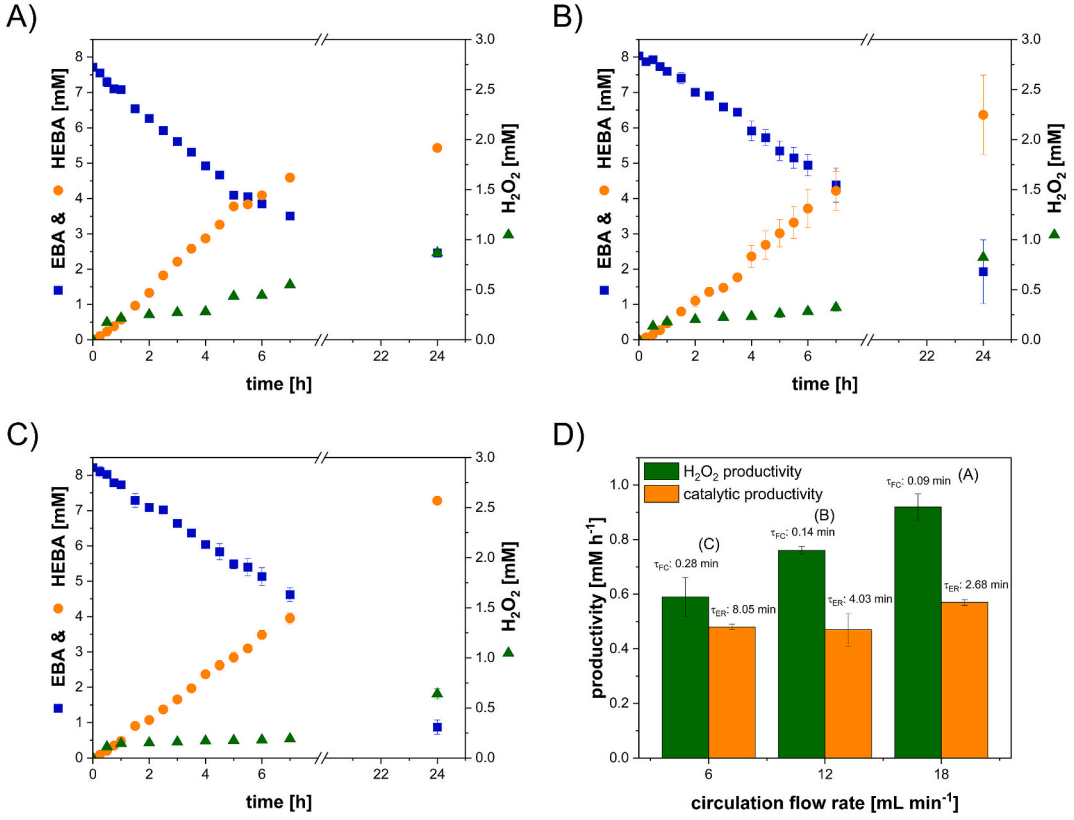

Fig. 6. Hydroxylation of EBA catalyzed by immobilized r*Aae*UPO in a circulation loop reactor equipped with the All-in-One electrode for *in situ* H_2O_2 generation at A) a circulation flow rate of 18 mL min^{-1} (resulting τ_{FC}: 0.09 min and τ_{ER}: 2.68 min), B) a circulation flow rate of 12 mL min^{-1}(resulting τ_{FC}: 0.14 min and τ_{ER}: 4.03 min) and C) a circulation flow rate of 6 mL min^{-1} (resulting τ_{FC}: 0.28 min and τ_{ER}: 8.05 min). D) Specific H_2O_2 productivity and catalytic productivity as a function of circulation flow rate (depicted τ_{FC} and τ_{ER} are the corresponding resulting residence time in the flow cell and enzyme reactor based on the set circulation flow rate). Conditions: 50 mL 0.1 M KP_i pH 7, 8 mM EBA, 0.8 g carrier (40 nM r*Aae*UPO), 1000 rpm, 0.61 mA cm^{-2}, 4 vvm and at 22 ± 1 °C. EBA: 4-ethylbenzoic acid, HEBA: 4-(1-hydroxyethyl)benzoic acid. Duplicates were performed.

3.3. Evaluation of different residence times and fed-batch operation mode on electroenzymatic hydroxylation

Once the implementation of the AiO electrode in a BES, specifically in a flow cell of the circulation loop reactor, was established, the next step was to evaluate the effect of the residence time on the electroenzymatic hydroxylation. This investigation was accomplished by employing different circulation flow rates within the pump's limits, which resulted in varying residence time in both flow cell (τ_{FC}) and enzyme reactor (τ_{ER}).

Electroenzymatic hydroxylation at different residence times was performed at 0.61 mA cm^{-2} because, based on previous results, this current density delivered one of the highest final HEBA concentration and TTN (Table. 1), as well as the highest F.E. in this study (Fig. 3**. C**). The tested circulation flow rates were 6 mL min^{-1}, 12 mL min^{-1} and 18 mL min^{-1}, which corresponded to τ_{FC} of 0.28 min, 0.14 min and 0.09 min, and to τ_{ER} of 8.05 min, 4.03 min and 2.68 min, respectively. The results from this investigation are shown in Fig. 6. Simultaneously, the corresponding performance indicators are listed in Table 2.

As shown in Fig. 6, the apparent accumulation of H_2O_2 decreases as the τ_{FC} increases (circulation flow rate decreases). At the highest τ_{FC} tested, 0.28 min (circulation flow rate: 6 mL min^{-1}), the accumulation of H_2O_2 was less than 0.2 mM after 7 h. Consequently, with lower productivity and accumulation of H_2O_2 in the medium, the operational stability of r*Aae*UPO was higher, resulting in higher final HEBA concentration and TTN (Table 2). The highest final concentration of HEBA and TTN in this regard were 7.28 ± 0.05 mM and $1.76 \cdot 10^5$ ± 1,213 mol mol^{-1}, respectively. Although a trend was observed for the TOF, with a slight increase as the τ_{FC} decreased, this change was not substantial. The resulting TOF from all the experiments were close to each other, and this can be explained by the fact that the experiments were run at a concentration of H_2O_2 well below its reported K_M value ($K_{M,\ H2O2}$: 0.79–1.8 mM [37,49,74]) to make a substantial difference in the catalytic rate. Furthermore, Fig. 6**. D** shows the catalytic productivity and the specific H_2O_2 productivity (in the absence of simultaneous biocatalytic reaction) as a function of the circulation flow rate. Consistent with previous observations (Fig. 4**. C**), H_2O_2 productivity increases with higher circulation flow rates or shorter residence time. This enhancement is attributed to improved oxygen mass transfer rate to the cathode, faster desorption of formed H_2O_2 from the cathode and thinner electrochemical double layer at the cathode interface. Although the catalytic productivity follows a similar trend, it is consistently around 19–38 % lower than their corresponding H_2O_2 productivity, leading to a H_2O_2 accumulation in the medium over time. This difference indicates that, in this specific system and under selected conditions, the catalytic productivity in the enzyme reactor is the rate limiting step, rather than the H_2O_2 productivity. This contrasts with the BES employing free r*Aae*UPO [44], where the H_2O_2 productivity was the limiting factor. A lower catalytic productivity observed in this study could be explained by two main reasons. First, the application of immobilized r*Aae*UPO likely reduces the enzyme activity compared to free enzymes due to steric hindrance or mass transport limitations of either the substrate EBA or the co-substrate H_2O_2. Second, the resulting τ_{ER} might still be too low, meaning that there was insufficient residence time in the enzyme reactor for the biocatalytic reaction to fully proceed and consumed the formed H_2O_2. To offset the imbalance between the H_2O_2 productivity and the catalytic productivity the τ_{ER} could be increased by increasing the volume of the enzyme reactor while keeping the τ_{FC} constant, applying a lower circulation flow rate (resulting in higher τ_{FC} and τ_{ER}) to further reduce the H_2O_2 productivity, or by increasing the applied enzyme concentration. In summary, these results suggest that applying a low current density in combination with a low circulation flow rate, resulting in high τ_{FC} and τ_{ER}, is beneficial for minimizing H_2O_2 accumulation in the reaction medium and achieving a high TTN. However, it is important to note that this combination also results in relatively low TOF and F.E., primarily due to reduced oxygen mass transfer to the cathode, slower desorption of the generated H_2O_2, and an increased thickness of the electrochemical double layer, as previously discussed.

Under current operating conditions, the TTN of r*Aae*UPO in the hydroxylation of EBA was limited by the initial EBA concentration and the concentration of r*Aae*UPO, which were 8 mM and 40 nM, respectively. To increase the efficiency of the system and the TTN, the experiment could be performed with a higher initial EBA concentration. However, the activity of r*Aae*UPO decreases at an EBA concentration higher than 8 mM due to substrate surplus inhibition (**Fig. S9**). Therefore, the electroenzymatic experiment was conducted under an EBA fed-batch operation mode. By continuously feeding highly concentrated EBA solution (200 mM) into the medium, the concentration of EBA could be maintained well above its K_M value ($K_{M,\ EBA}$: 2.3 mM [37]). This may not only increase the catalytic rate, it may also minimize the catalase malfunction reaction. Given the high concentration of EBA employed in the fed-batch operation mode, the reaction volume increased only by a maximum of 1.7 mL. The increase in reaction volume resulting from the feeding was counterbalanced by the sampling and volume loss due to evaporation caused by sparging, which were subsequently taken into account for the calculation of the concentrations. The results for the electroenzymatic hydroxylation of EBA under the EBA fed-batch operation mode are depicted in Fig. 7.

EBA feeding was started after 90 min of the start of the reaction. To avoid an accumulation of EBA way above 8 mM, the feeding rate was set to 0.008–0.016 mmol h^{-1} (0.16–0.32 mM h^{-1}), which was lower than the actual catalytic rate determined from previous experiment (Fig. 6**. C**). The fed-batch operation mode was able to maintain the EBA concentration between 6 mM and 9 mM during the whole duration of the experiment. Nevertheless, the EBA concentration was increasing near the end of the experiment because the activity of the enzyme was decreasing and correspondingly, the EBA conversion rate as well. The continuous supply of substrate EBA increased the catalytic productivity by 20.8 %, from 0.48 ± 0.01 mM h^{-1} (Table 2) to 0.58 ± 0.02 mM h^{-1} (Table 3). At the same time, the final HEBA concentration and the TTN obtained under the fed-batch operation mode were elevated to 10.43 ± 0.24 mM and $2.53 \cdot 10^5$ ± 5,887 mol mol^{-1}, respectively, in comparison

Table 2
Summary of total turnover number (TTN), turnover frequency (TOF), catalytic productivity and final concentration of HEBA determined from electroenzymatic experiments in the circulation loop reactor equipped with the All-in-One electrode at various residence times, at 0.61 mA cm^{-2}.

τ_{FC} (τ_{ER}) [min]	catalytic productivity [mM h^{-1}]	final HEBA concentration [mM]	TOF [s^{-1}]	TTN [mol mol^{-1}]
0.28 (8.05)	0.48 ± 0.01	7.28 ± 0.05	3.24 ± 0.09	$1.76 \cdot 10^5$ ± 1,213
0.14 (4.03)	0.47 ± 0.06	6.37 ± 1.12	3.14 ± 0.44	$1.54 \cdot 10^5$ ± 27,234
0.09 (2.68)	0.57 ± 0.01	5.43 ± 0.04	3.85 ± 0.04	$1.31 \cdot 10^5$ ± 970

τ_{FC}: resulting residence time in the flow cell. τ_{ER}: resulting residence time in the enzyme reactor. τ_{FC} of 0.28 min, 0.14 min and 0.09 min correspond to circulation flow rates of 6 mL min^{-1}, 12 mL min^{-1} and 18 mL min^{-1}, respectively. τ_{ER} of 8.05 min, 4.03 min and 2.68 min correspond to circulation flow rates of 6 mL min^{-1}, 12 mL min^{-1} and 18 mL min^{-1}, respectively. Conditions: 50 mL 0.1 M KP_i pH 7, 8 mM EBA, 0.8 g carrier (40 nM r*Aae*UPO), 1000 rpm, 0.61 mA cm^{-2}, 4 vvm and at 22 ± 1 °C. Duplicates were performed.

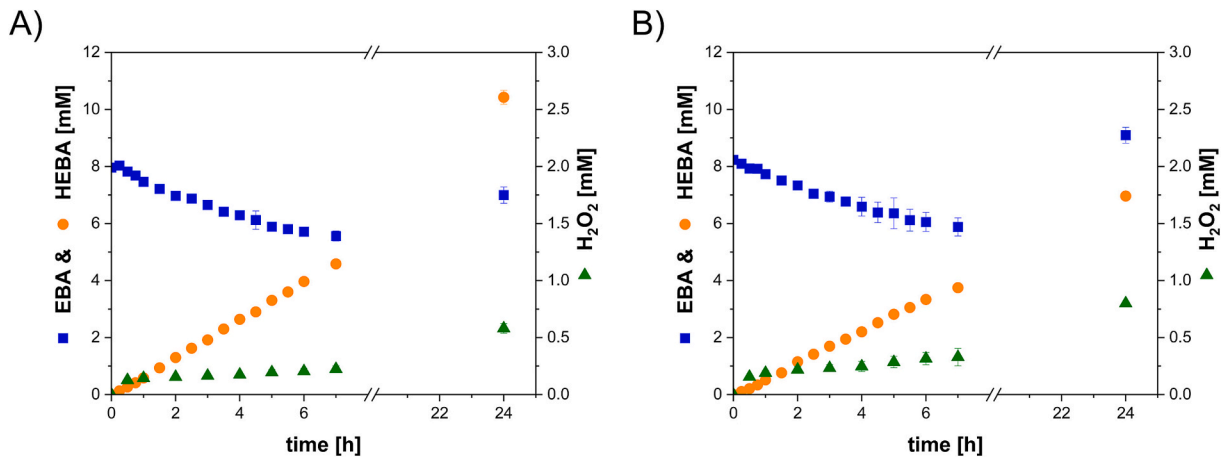

Fig. 7. Hydroxylation of EBA catalyzed by immobilized r*Aae*UPO in a circulation loop reactor equipped with the All-in-One electrode for *in situ* H_2O_2 generation. A) Fed-batch operation mode with 0.8 g carrier (40 nM r*Aae*UPO). B) Fed-batch operation mode with 0.4 g carrier (20 nM r*Aae*UPO). Conditions: 50 mL 0.1 M KP_i pH 7, 8 mM EBA, 1000 rpm, circulation flow rate: 6 mL min^{-1} (resulting τ_{FC}: 0.28 min and τ_{ER}: 8.05 min), 0.61 mA cm^{-2}, 4 vvm, 200 mM EBA stock solution and at 22 ± 1 °C. EBA: 4-ethylbenzoic acid, HEBA: 4-(1-hydroxyethyl)benzoic acid. Duplicates were performed.

Table 3
Summary of total turnover number (TTN), turnover frequency (TOF), catalytic productivity and final concentration of HEBA determined from electroenzymatic experiments in the circulation loop reactor equipped with the All-in-One electrode under fed-batch operation mode, and at various catalyst loading.

catalyst loading [g]	catalytic productivity [mM h^{-1}]	final HEBA concentration [mM]	TOF [s^{-1}]	TTN [mol mol^{-1}]
0.4	0.51 ± 0.05	6.96 ± 0.01	6.94 ± 0.70	$3.38 \cdot 10^5$ ± 702
0.8	0.58 ± 0.02	10.43 ± 0.24	3.93 ± 0.15	$2.53 \cdot 10^5$ ± 5,887

Conditions: 50 mL 0.1 M KP_i pH 7, 8 mM EBA, 1000 rpm, circulation flow rate: 6 mL min^{-1} (resulting τ_{FC}: 0.28 min and τ_{ER}: 8.05 min), 0.61 mA cm^{-2}, 4 vvm, 200 mM EBA stock solution and at 22 ± 1 °C. Duplicates were performed.

to the batch operation mode. To further enhance the catalyst efficiency, an electroenzymatic experiment was conducted using half of the catalyst loading, corresponding to 0.4 g. This approach was supported by the observation that by adjusting the current density and the residence time, the accumulation of H_2O_2 could be maintained at approximately 0.2 mM (Fig. 6. **C**, Fig. 7. **A**). Thus, despite the reduced catalyst loading, the enzyme stability could be conserved for a longer time.

The reduction in the catalyst loading resulted in a 12 % decline in catalytic productivity, from 0.58 ± 0.02 mM h^{-1} to 0.51 ± 0.05 mM h^{-1}. As a consequence of the reduced catalyst loading, the H_2O_2 consumption rate decreased, resulting in a higher accumulation of H_2O_2 within the medium, reaching approximately 0.3 mM after 7 h. In addition to the reduced catalyst loading, the higher accumulation of H_2O_2 also led to a faster enzyme deactivation. Accordingly, the final concentration of HEBA was lower, at 6.96 ± 0.01 mM. Nevertheless, the obtained TTN using 50 % less catalyst loading was 33 % higher, with a value of $3.38 \cdot 10^5$ ± 702 mol mol^{-1}. It is possible that a further reduction in catalyst loading may not necessarily increase the TTN substantially. This is because the rate of H_2O_2 production may exceed the rate of enzymatic conversion of H_2O_2, resulting in a higher accumulation.

A TTN value of $3.38 \cdot 10^5$ ± 702 mol mol^{-1} is comparable to those reported in the literature for BES employing electrochemical generation of H_2O_2, which range from $1.45 \cdot 10^5$ mol mol^{-1} to $6.5 \cdot 10^5$ mol mol^{-1} (Table 4) [29,35,37,40,76]. It is also comparable to the TTN reported for a system utilizing the AiO electrode in a stirred tank reactor ($4.5 \cdot 10^5$ mol mol^{-1}) [44] and exceeds the TTN obtained in the system employing manual addition of H_2O_2 ($1.64 \cdot 10^5$ mol mol^{-1}) [69]. In comparison to a system employing an enzymatic cascade for *in situ* generation of H_2O_2, which reported a TTN of $4.7 \cdot 10^5$ mol mol^{-1} [77], the TTN achieved here is 28 % lower. However, to realize such an enzymatic cascade, five different enzymes, NAD^+ as a cofactor, and methanol as a sacrificial electron donor were required [77]. It is important to note that the immobilization might introduce the possibility of steric hindrance, diffusion limitations, or multi-layer adsorption on the carrier. To counteract these effects, up to 4 times higher enzyme concentration was used in this study compared to the system utilizing free enzyme [76]. Although similar final product concentrations were achieved, the resulting TTN here is lower due to the higher enzyme loading [76]. In terms of the TOF, a TOF of 8.34 ± 0.14 s^{-1} is approximately 14 times lower than the TOF reported in a gas diffusion electrode (GDE) system [37]. This is due to the lower H_2O_2 productivities achieved in this system in comparison to those observed in GDE-based systems [35–37,40]. Nonetheless, both system's productivity and TOF could be enhanced by implementing numbering-up or modular stacking of the flow cell to

Table 4
Comparison of total turnover number (TTN) achieved in this study with values reported in the literature.

Substrate, enzyme	Reaction system	TTN [mol mol^{-1}]	Ref.
Thioanisole, CPO	Batch process, in a three dimensional electrochemical cell using graphite grains as cathode	$1.45 \cdot 10^5$	[29]
Monochlordimedone, CPO	Fed-batch process, in a GDE-based electrochemical system	$2.03 \cdot 10^5$	[35]
EBA, r*Aae*UPO	Batch process, in a GDE-based electrochemical system	$4.00 \cdot 10^5$	[37]
Ethylbenzene, r*Aae*UPO	Batch process, in a GDE-based electrochemical system	$4.00 \cdot 10^5$	[40]
EBA, r*Aae*UPO	Batch process, in a GDE-based electrochemical system	$6.50 \cdot 10^5$	[76]
EBA, r*Aae*UPO	Batch process, in an AiO electrode system	$4.50 \cdot 10^5$	[44]
EBA, r*Aae*UPO	Batch process, using manual addition of H_2O_2	$1.64 \cdot 10^5$	[69]
Ethylbenzene, r*Aae*UPO	Batch process, using enzymatic *in situ* generation of H_2O_2	$4.70 \cdot 10^5$	[77]
EBA, r*Aae*UPO	Fed-batch process, using immobilized r*Aae*UPO in an electrochemical flow cell	$3.38 \cdot 10^5$	This study

increase surface to volume ratio, as well as surface modification of the cathode to increase the H_2O_2 selectivity.

4. Conclusions

The AiO electrode was successfully integrated within an electrochemical flow cell to enable the electrochemical *in situ* generation of H_2O_2. The feasibility of this concept was validated through an electroenzymatic hydroxylation catalyzed by immobilized r*Aae*UPO, utilizing H_2O_2 as the cosubstrate. Electroenzymatic experiments under batch and fed-batch operation modes were performed. The results indicated that within a flow cell, not only do current density, cell potential and aeration rate significantly influence H_2O_2 productivity and its accumulation, but the residence time (flow rate) is also critical. This is because the aforementioned parameters influence the reaction rate of competing reactions, availability of oxygen in the medium, mass transfer of oxygen towards the cathode, desorption of formed H_2O_2 from the cathode and thickness of electrochemical double layer. Moreover, the containment of the carrier within the SpinChem® MagRBR facilitated a simple separation of the biocatalyst from the reaction medium. The study achieved a TTN comparable to the best values reported in the literature within a BES. Within the system, the electrochemical *in situ* generation of H_2O_2 proved to be an effective method for minimizing biocatalyst deactivation by ensuring a controllable supply of H_2O_2 and preventing its excessive accumulation. This implementation demonstrates the potential for flow reactor technology in BES to facilitate alternative scale-up strategies, such as numbering-up or modular stacking. This aspect will be investigated further in a subsequent study, in which the flow cell will be operated continuously, either in a plug flow mode or in a continuous stirred tank reactor mode. Further optimization of the flow cell BES is ongoing, particularly regarding H_2O_2 productivity and Faradaic efficiency (F.E.). Potential enhancements include surface modification approaches, such as coating with carbon nanotubes, surface oxidation and thermal treatment. Additionally, the system's applicability could be broadened by employing industrially relevant model reactions, such as the oxidation of 5-(hydroxymethyl)furfural to 2,5-furandicarboxylic acid. This study demonstrates that the integration of the AiO electrode within flow reactor technology is not only feasible but also offers a promising alternative scalable strategy. It provides a reliable platform for H_2O_2-dependent enzymatic reactions, paving the way for further advancements in the field.

CRediT authorship contribution statement

Giovanni V. Sayoga: Writing – original draft, Visualization, Validation, Investigation, Formal analysis, Data curation. **Victoria S. Bueschler:** Writing – review & editing, Validation, Investigation. **Hubert Beisch:** Writing – review & editing. **Bodo Fiedler:** Writing – review & editing, Funding acquisition. **Daniel Ohde:** Writing – review & editing, Supervision, Project administration. **Andreas Liese:** Writing – review & editing, Supervision, Resources, Funding acquisition, Data curation, Conceptualization.

Declaration of generative AI and AI-assisted technologies in the writing process

During the preparation of this work the author(s) used ChatGPT in order to improve the readability. After using this tool, the author(s) reviewed and edited the content as needed and take(s) full responsibility for the content of the publication.

Declaration of competing interest

The authors declare that they have no known competing financial interests or personal relationships that could have appeared to influence the work reported in this paper.

Acknowledgements

This work was supported by the Deutsche Forschungsgemeinschaft (DFG, German Research Foundation, e-Biotech SPP 2240) (Project number: 445947004). Publishing fees supported by Funding Program Open Access Publishing of Hamburg University of Technology (TUHH). The authors thank Prof. Dirk Holtmann of the Karlsruhe Institute of Technology for providing the *Pichia pastoris* (X33) strain, expressing the recombinant protein r*Aae*UPO-PaDa-I-C6His. Furthermore, the authors thank SpinChem for providing the SpinChem® magnetic rotating bed reactor. Finally, the authors thank Fernando Lopez Haro of the Hamburg University of Technology for the preparation of the graphical abstract.

Appendix A. Supplementary data

Supplementary data to this article can be found online at https://doi.org/10.1016/j.elecom.2025.107949.

Data availability

Data will be made available on request.

References

[1] C.B. Chidambara Raj, H. Li Quen, Advanced oxidation processes for wastewater treatment: optimization of UV/H_2O_2 process through a statistical technique, Chem. Eng. Sci. 60 (2005) 5305–5311, https://doi.org/10.1016/j.ces.2005.03.065.
[2] M.A. Camblor, A. Corma, A. Martínez, J. Pérez-Pariente, Synthesis of a titaniumsilicoaluminate isomorphous to zeolite beta and its application as a catalyst for the selective oxidation of large organic molecules, J. Chem. Soc. Chem. Commun. 0 (1992) 589–590, https://doi.org/10.1039/C39920000589.
[3] M.G. Clerici, P. Ingallina, Epoxidation of lower olefins with hydrogen peroxide and titanium silicalite, J. Catal. 140 (1993) 71–83, https://doi.org/10.1006/jcat.1993.1069.
[4] K. Kosaka, H. Yamada, K. Shishida, S. Echigo, R.A. Minear, H. Tsuno, S. Matsui, Evaluation of the treatment performance of a multistage ozone/hydrogen peroxide process by decomposition by-products, Water Res. 35 (2001) 3587–3594, https://doi.org/10.1016/S0043-1354(01)00087-2.
[5] Y.L. Hsiao, K. Nobe, Oxidative reactions of phenol and chlorobenzene with *in situ* electrogenerated Fenton's reagent, Chem. Eng. Commun. 126 (1993) 97–110, https://doi.org/10.1080/00986449308936212.
[6] H. Li, E. Quispe-Cardenas, S. Yang, L. Yin, Y. Yang, Electrosynthesis of >20 g/L H_2O_2 from air, ACS EST Eng. 2 (2022) 242–250, https://doi.org/10.1021/acsestengg.1c00366.
[7] J.M. Campos-Martin, G. Blanco-Brieva, J.L. Fierro, Hydrogen peroxide synthesis: an outlook beyond the anthraquinone process, Angew. Chem. Int. Ed. 45 (2006) 6962–6984.
[8] Z. Pan, K. Wang, Y. Wang, P. Tsiakaras, S. Song, *In-situ* electrosynthesis of hydrogen peroxide and wastewater treatment application: a novel strategy for graphite felt activation, Appl. Catal. B Environ. 237 (2018) 392–400, https://doi.org/10.1016/j.apcatb.2018.05.079.
[9] J.S.J. Hargreaves, Y.-M. Chung, W.-S. Ahn, T. Hisatomi, K. Domen, M.C. Kung, H. H. Kung, Minimizing energy demand and environmental impact for sustainable NH_3 and H_2O_2 production—a perspective on contributions from thermal, electro-, and photo-catalysis, Appl. Catal. A Gen. 594 (2020) 117419, https://doi.org/10.1016/j.apcata.2020.117419.
[10] Q. Jiang, Y. Ji, T. Zheng, X. Li, C. Xia, The Nexus of innovation: electrochemically synthesizing H_2O_2 and its integration with downstream reactions, ACS Mater. Au 4 (2024) 133–147, https://doi.org/10.1021/acsmaterialsau.3c00070.
[11] M. Qiao, X. Zhou, Z. Du, P. Wu, B. Zong, Chemical and engineering bases for green H_2O_2 production and related oxidation and ammoximation of olefins and analogues, Natl. Sci. Rev. 11 (2024) nwae243, https://doi.org/10.1093/nsr/nwae243.
[12] J.K. Edwards, G.J. Hutchings, Palladium and gold–palladium catalysts for the direct synthesis of hydrogen peroxide, Angew. Chem. Int. Ed. 47 (2008) 9192–9198, https://doi.org/10.1002/anie.200802818.
[13] M.J. Palmer, A.J. Musker, G.T. Roberts, C.A. Ponce de Leon Albarran, A method of ranking candidate catalyst for the decomposition of hydrogen peroxide. https://eprints.soton.ac.uk/170997/, 2010 (accessed April 25, 2024).
[14] M. Ventura, S. Yuan, Commercial production and use of hydrogen peroxide, In: 36th AIAAASMESAEASEE Jt. Propuls. Conf. Exhib., American Institute of Aeronautics and Astronautics, Las Vegas,NV,U.S.A, 2000, https://doi.org/10.2514/6.2000-3556.
[15] J. Zhou, H. Guo, X. Wang, M. Guo, J. Zhao, L. Chen, W. Gong, Direct and continuous synthesis of concentrated hydrogen peroxide by the gaseous reaction of H_2/O_2 non-equilibrium plasma, Chem. Commun. 0 (2005) 1631–1633, https://doi.org/10.1039/B416835F.
[16] P. Landon, P.J. Collier, A.F. Carley, D. Chadwick, A.J. Papworth, A. Burrows, C. J. Kiely, G.J. Hutchings, Direct synthesis of hydrogen peroxide from H_2 and O_2

using Pd and au catalysts, Phys. Chem. Chem. Phys. 5 (2003) 1917–1923, https://doi.org/10.1039/B211338B.
[17] S.C. Perry, D. Pangotra, L. Vieira, L.-I. Csepei, V. Sieber, L. Wang, C. Ponce de León, F.C. Walsh, Electrochemical synthesis of hydrogen peroxide from water and oxygen, Nat. Rev. Chem. 3 (2019) 442–458.
[18] B.O. Burek, S. Bormann, F. Hollmann, J.Z. Bloh, D. Holtmann, Hydrogen peroxide driven biocatalysis, Green Chem. 21 (2019) 3232–3249, https://doi.org/10.1039/C9GC00633H.
[19] H.L. Wapshott-Stehli, A.M. Grunden, *In situ* H_2O_2 generation methods in the context of enzyme biocatalysis, Enzym. Microb. Technol. 145 (2021) 109744, https://doi.org/10.1016/j.enzmictec.2021.109744.
[20] S. Peter, M. Kinne, R. Ullrich, G. Kayser, M. Hofrichter, Epoxidation of linear, branched and cyclic alkenes catalyzed by unspecific peroxygenase, Enzym. Microb. Technol. 52 (2013) 370–376, https://doi.org/10.1016/j.enzmictec.2013.02.013.
[21] S. Kern, A. Himmelspach, K. Grammann, O. Thum, A. Liese, Process characterization studies for solvent-free simultaneous epoxidation and transesterification of fatty acid methyl esters, Org. Process. Res. Dev. 20 (2016) 1930–1936, https://doi.org/10.1021/acs.oprd.6b00254.
[22] C.E. Wise, C.H. Hsieh, N.L. Poplin, T.M. Makris, Dioxygen activation by the biofuel-generating cytochrome P450 OleT, ACS Catal. 8 (2018) 9342–9352, https://doi.org/10.1021/acscatal.8b02631.
[23] A. Karich, M. Kluge, R. Ullrich, M. Hofrichter, Benzene oxygenation and oxidation by the peroxygenase of *Agrocybe aegerita*, AMB Express 3 (2013) 5, https://doi.org/10.1186/2191-0855-3-5.
[24] J.-B. Park, D.S. Clark, Deactivation mechanisms of chloroperoxidase during biotransformations, Biotechnol. Bioeng. 93 (2006) 1190–1195, https://doi.org/10.1002/bit.20825.
[25] M. Abt, M. Franzreb, M. Jestädt, A. Tschöpe, Three-phase fluidized bed electrochemical reactor for the scalable generation of hydrogen peroxide at enzyme compatible conditions, Chem. Eng. J. 476 (2023) 146465, https://doi.org/10.1016/j.cej.2023.146465.
[26] S. Bormann, A.G. Baraibar, Y. Ni, D. Holtmann, F. Hollmann, Specific oxyfunctionalisations catalysed by peroxygenases: opportunities, challenges and solutions, Catal. Sci. Technol. 5 (2015) 2038–2052, https://doi.org/10.1039/C4CY01477D.
[27] C. Kohlmann, S. Lütz, Electroenzymatic synthesis of chiral sulfoxides, Eng. Life Sci. 6 (2006) 170–174, https://doi.org/10.1002/elsc.200620907.
[28] K. Seelbach, M.P.J. van Deurzen, F. van Rantwijk, R.A. Sheldon, U. Kragl, Improvement of the total turnover number and space-time yield for chloroperoxidase catalyzed oxidation, Biotechnol. Bioeng. 55 (1997) 283–288, https://doi.org/10.1002/(SICI)1097-0290(19970720)55:2<283::AID-BIT6>3.0.CO;2-E.
[29] S. Lütz, K. Vuorilehto, A. Liese, Process development for the electroenzymatic synthesis of (*R*)-methylphenylsulfoxide by use of a 3-dimensional electrode, Biotechnol. Bioeng. 98 (2007) 525–534, https://doi.org/10.1002/bit.21434.
[30] F. van Rantwijk, R.A. Sheldon, Selective oxygen transfer catalysed by heme peroxidases: synthetic and mechanistic aspects, Curr. Opin. Biotechnol. 11 (2000) 554–564, https://doi.org/10.1016/S0958-1669(00)00143-9.
[31] P. Zhou, J. Zhang, Y. Zhang, Y. Liu, J. Liang, B. Liu, W. Zhang, Generation of hydrogen peroxide and hydroxyl radical resulting from oxygen-dependent oxidation of L-ascorbic acid via copper redox-catalyzed reactions, RSC Adv. 6 (2016) 38541–38547, https://doi.org/10.1039/C6RA02843H.
[32] M.A. Matthews, Green electrochemistry. Examples and challenges, Pure Appl. Chem. 73 (2001) 1305–1308.
[33] G. Sayoga, M. Abt, N. Teetz, V. Bueschler, A. Liese, M. Franzreb, D. Holtmann, Quantitative and non-quantitative assessments of enzymatic Electrosynthesis: a case study of parameter requirements, ChemElectroChem 10 (2023) e202300226, https://doi.org/10.1002/celc.202300226.
[34] D. Deng, Z. Jiang, L. Kang, L. Liao, X. Zhang, Y. Qiao, B. Wang, A. Li, Unravelling an Efficient O_2/Reductant-Dependent Catalytic Route in Heme Peroxygenases for Sustainable Applications, 2024, https://doi.org/10.1101/2024.05.25.595845, 2024.05.25.595845.
[35] T. Krieg, S. Hüttmann, K.-M. Mangold, J. Schrader, D. Holtmann, Gas diffusion electrode as novel reaction system for an electro-enzymatic process with chloroperoxidase, Green Chem. 13 (2011) 2686–2689, https://doi.org/10.1039/C1GC15391A.
[36] D. Holtmann, T. Krieg, L. Getrey, J. Schrader, Electroenzymatic process to overcome enzyme instabilities, Catal. Commun. 51 (2014) 82–85.
[37] S. Bormann, D. Hertweck, S. Schneider, J.Z. Bloh, R. Ulber, A.C. Spiess, D. Holtmann, Modeling and simulation-based design of electroenzymatic batch processes catalyzed by unspecific peroxygenase from *a. aegerita*, Biotechnol. Bioeng. 118 (2021) 7–16.
[38] S. Lütz, E. Steckhan, A. Liese, First asymmetric electroenzymatic oxidation catalyzed by a peroxidase, Electrochem. Commun. 6 (2004) 583–587, https://doi.org/10.1016/j.elecom.2004.04.009.
[39] S. Bormann, M.M. van Schie, T.P. De Almeida, W. Zhang, M. Stöckl, R. Ulber, F. Hollmann, D. Holtmann, H_2O_2 production at low overpotentials for electroenzymatic halogenation reactions, ChemSusChem 12 (2019) 4759–4763.
[40] A.E.W. Horst, S. Bormann, J. Meyer, M. Steinhagen, R. Ludwig, A. Drews, M. Ansorge-Schumacher, D. Holtmann, Electro-enzymatic hydroxylation of ethylbenzene by the evolved unspecific peroxygenase of *Agrocybe aegerita*, J. Mol. Catal. B Enzym. 133 (2016) S137–S142, https://doi.org/10.1016/j.molcatb.2016.12.008.
[41] T. Utesch, A.-P. Zeng, A novel all-in-one electrolysis electrode and bioreactor enable better study of electrochemical effects and electricity-aided bioprocesses, Eng. Life Sci. 18 (2018) 600–610.
[42] J. Herzog, A. Mook, L. Guhl, M. Bäumler, M.H. Beck, D. Weuster-Botz, F. R. Bengelsdorf, A.-P. Zeng, Novel synthetic co-culture of *Acetobacterium woodii* and *Clostridium drakei* using CO_2 and *in situ* generated H_2 for the production of caproic acid via lactic acid, Eng. Life Sci. 23 (2022) e2100169, https://doi.org/10.1002/elsc.202100169.
[43] P. Arbter, A. Sinha, J. Troesch, T. Utesch, A.-P. Zeng, Redox governed electro-fermentation improves lipid production by the oleaginous yeast *Rhodosporidium toruloides*, Bioresour. Technol. 294 (2019) 122122, https://doi.org/10.1016/j.biortech.2019.122122.
[44] G.V. Sayoga, V.S. Bueschler, H. Beisch, D. Holtmann, A.-P. Zeng, B. Fiedler, D. Ohde, A. Liese, Application of the all-in-one electrode for *in situ* H_2O_2 generation in hydroxylation catalyzed by unspecific peroxygenase from *Agrocybe aegerita*, Mol. Catal. 547 (2023) 113325, https://doi.org/10.1016/j.mcat.2023.113325.
[45] P. Watts, C. Wiles, Micro reactors, flow reactors and continuous flow synthesis, J. Chem. Res. 36 (2012) 181–193, https://doi.org/10.3184/174751912X13311365798808.
[46] I.R. Baxendale, The integration of flow reactors into synthetic organic chemistry, J. Chem. Technol. Biotechnol. 88 (2013) 519–552, https://doi.org/10.1002/jctb.4012.
[47] M. Hofrichter, R. Ullrich, Oxidations catalyzed by fungal peroxygenases, Curr. Opin. Chem. Biol. 19 (2014) 116–125, https://doi.org/10.1016/j.cbpa.2014.01.015.
[48] P. Molina-Espeja, E. Garcia-Ruiz, D. Gonzalez-Perez, R. Ullrich, M. Hofrichter, M. Alcalde, Directed evolution of unspecific peroxygenase from *Agrocybe aegerita*, Appl. Environ. Microbiol. 80 (2014) 3496–3507.
[49] P. Molina-Espeja, S. Ma, D.M. Mate, R. Ludwig, M. Alcalde, Tandem-yeast expression system for engineering and producing unspecific peroxygenase, Enzym. Microb. Technol. 73–74 (2015) 29–33, https://doi.org/10.1016/j.enzmictec.2015.03.004.
[50] N. Büscher, G.V. Sayoga, K. Rübsam, F. Jakob, U. Schwaneberg, S. Kara, A. Liese, Biocatalyst immobilization by anchor peptides on an additively Manufacturable material, Org. Process. Res. Dev. 23 (2019) 1852–1859, https://doi.org/10.1021/acs.oprd.9b00152.
[51] Invitrogen, *Pichia* fermentation process guidelines. https://tools.thermofisher.com/content/sfs/manuals/pichiaferm_prot.pdf, 2002 accessed May 22, 2023.
[52] J. Cino, High-yield protein production from *Pichia pastoris* yeast: a protocol for benchtop fermentation, Am. Biotechnol. Lab. 17 (1999) 10–13.
[53] F. Perz, S. Bormann, R. Ulber, M. Alcalde, P. Bubenheim, F. Hollmann, D. Holtmann, A. Liese, Enzymatic oxidation of butane to 2-butanol in a bubble column, ChemCatChem 12 (2020) 3666–3669.
[54] A.R. Khataee, M. Safarpour, M. Zarei, S. Aber, Electrochemical generation of H_2O_2 using immobilized carbon nanotubes on graphite electrode fed with air: investigation of operational parameters, J. Electroanal. Chem. 659 (2011) 63–68, https://doi.org/10.1016/j.jelechem.2011.05.002.
[55] http://www.tinyblog.cn/wp-content/uploads/2021/06/Lifetech-Enzyme-Immobilization-Procedures.pdf, (2025). http://www.tinyblog.cn/wp-content/uploads/2021/06/Lifetech-Enzyme-Immobilization-Procedures.pdf (accessed January 19, 2025).
[56] Z. Perçin, L. Kursula, E. Löfgren, E. Byström, F. Kexel, P. Bubenheim, M. Schlüter, A. Liese, Intensification of a biocatalytic oxidation under fine bubble aeration in a rotating bed reactor, Biochem. Eng. J. 207 (2024) 109333, https://doi.org/10.1016/j.bej.2024.109333.
[57] E. Petrucci, A. Da Pozzo, L. Di Palma, On the ability to electrogenerate hydrogen peroxide and to regenerate ferrous ions of three selected carbon-based cathodes for electro-Fenton processes, Chem. Eng. J. 283 (2016) 750–758, https://doi.org/10.1016/j.cej.2015.08.030.
[58] G.A. Kolyagin, V.L. Kornienko, Pilot laboratory electrolyzer for electrosynthesis of hydrogen peroxide in acid and alkaline solutions, Russ. J. Appl. Chem. 84 (2011) 68–71, https://doi.org/10.1134/S1070427211010113.
[59] J.F. Pérez, A. Galia, M.A. Rodrigo, J. Llanos, S. Sabatino, C. Sáez, B. Schiavo, O. Scialdone, Effect of pressure on the electrochemical generation of hydrogen peroxide in undivided cells on carbon felt electrodes, Electrochim. Acta 248 (2017) 169–177, https://doi.org/10.1016/j.electacta.2017.07.116.
[60] E. Peralta, R. Natividad, G. Roa, R. Marin, R. Romero, T. Pavon, A comparative study on the electrochemical production of H_2O_2 between BDD and graphite cathodes, Sustain. Environ. Res. 23 (2013) 259–266.
[61] M. Panizza, G. Cerisola, Electrochemical generation of H_2O_2 in low ionic strength media on gas diffusion cathode fed with air, Electrochim. Acta 54 (2008) 876–878.
[62] K. Jüttner, Technical scale of electrochemistry, in: A.J. Bard (Ed.), Encycl. Electrochem, 1st ed, Wiley, 2007, https://doi.org/10.1002/9783527610426.bard050001.
[63] Z. Qiang, J.-H. Chang, C.-P. Huang, Electrochemical generation of hydrogen peroxide from dissolved oxygen in acidic solutions, Water Res. 36 (2002) 85–94.
[64] M. Sudoh, H. Kitaguchi, K. Koide, Electrochemical production of hydrogen peroxide by reduction of oxygen, J. Chem. Eng. Jpn 18 (1985) 409–414.
[65] Y. Sun, I. Sinev, W. Ju, A. Bergmann, S. Dresp, S. Kühl, C. Spöri, H. Schmies, H. Wang, D. Bernsmeier, B. Paul, R. Schmack, R. Kraehnert, B. Roldan Cuenya, P. Strasser, Efficient electrochemical hydrogen peroxide production from molecular oxygen on nitrogen-doped mesoporous carbon catalysts, ACS Catal. 8 (2018) 2844–2856, https://doi.org/10.1021/acscatal.7b03464.
[66] A.D. Pozzo, L.D. Palma, C. Merli, E. Petrucci, An experimental comparison of a graphite electrode and a gas diffusion electrode for the cathodic production of hydrogen peroxide, J. Appl. Electrochem. 35 (2005) 413–419, https://doi.org/10.1007/s10800-005-0800-2.

[67] J.K. Chen, K. Nobe, Oxidation of dimethylaniline by horseradish peroxidase and electrogenerated peroxide: I. Free enzyme studies, J. Electrochem. Soc. 140 (1993) 299, https://doi.org/10.1149/1.2221041.
[68] K. Wang, Z. Zhu, D. Xu, M. Li, S. Yuan, H. Wang, Highly active and cheap graphite/polytetrafluoroethylene composite coating cathodes for electrogeneration of hydrogen peroxide, Clean Techn. Environ. Policy 24 (2022) 2407–2417, https://doi.org/10.1007/s10098-022-02323-z.
[69] S. Bormann, B.O. Burek, R. Ulber, D. Holtmann, Immobilization of unspecific peroxygenase expressed in *Pichia pastoris* by metal affinity binding, Mol. Catal. 492 (2020) 110999, https://doi.org/10.1016/j.mcat.2020.110999.
[70] D. Arnold, C. Plank, E. Erickson, F. Pike, Solubility of benzene in water, Ind. Eng. Chem. Chem. Eng. Data Ser. 3 (1958) 253–256, https://doi.org/10.1021/i460004a016.
[71] Ethylbenzene (EHC 186, 1996). https://www.inchem.org/documents/ehc/ehc/ehc186.htm, 2025 accessed January 19, 2025.
[72] M. Hobisch, P. De Santis, S. Serban, A. Basso, E. Byström, S. Kara, Peroxygenase-driven ethylbenzene hydroxylation in a rotating bed reactor, Org. Process. Res. Dev. 26 (2022) 2761–2765.
[73] N. Büscher, C. Spille, J.K. Kracht, G.V. Sayoga, A.W.H. Dawood, M.I. Maiwald, D. Herzog, M. Schlüter, A. Liese, Countercurrently operated reactive extractor with an additively manufactured enzyme carrier structure, Org. Process. Res. Dev. 24 (2020) 1621–1628, https://doi.org/10.1021/acs.oprd.0c00205.
[74] A. Karich, K. Scheibner, R. Ullrich, M. Hofrichter, Exploring the catalase activity of unspecific peroxygenases and the mechanism of peroxide-dependent heme destruction, J. Mol. Catal. B Enzym. 134 (2016) 238–246, https://doi.org/10.1016/j.molcatb.2016.10.014.
[75] P. De Santis, N. Petrovai, L.-E. Meyer, M. Hobisch, S. Kara, A holistic carrier-bound immobilization approach for unspecific peroxygenase, Front. Chem. 10 (2022), https://doi.org/10.3389/fchem.2022.985997.
[76] G.V. Sayoga, V.S. Bueschler, H. Beisch, T. Utesch, D. Holtmann, B. Fiedler, D. Ohde, A. Liese, Electrochemical H_2O_2-stat mode as reaction concept to improve the process performance of an unspecific peroxygenase, New Biotechnol. 78 (2023) 95–104, https://doi.org/10.1016/j.nbt.2023.10.007.
[77] Y. Ni, E. Fernández-Fueyo, A.G. Baraibar, R. Ullrich, M. Hofrichter, H. Yanase, M. Alcalde, W.J.H. van Berkel, F. Hollmann, Peroxygenase-catalyzed oxyfunctionalization reactions promoted by the complete oxidation of methanol, Angew. Chem. Int. Ed. 55 (2016) 798–801, https://doi.org/10.1002/anie.201507881.